Pak.j.stat.oper.res. Vol.22 No. 3 2026 pp 473-500 DOI: http://dx.doi.org/10.18187/pjsor.v22i3.4903

Pakistan Journal of Statistics and Operation Research

A New Light-tailed Weighted Model for Reliability Risk Analysis: Theory, Properties and Case Study

Mohamed Ibrahim[1,*] , Gadir Alomair[1] , Abdussalam Aljadani[2], Mohamed Aboraya[3], Sami A. Morsi[4], Haitham M. Yousof[5], Mujtaba Hashim[1] and Rehab Shehata Mahmoud[5]

* Corresponding Author

[1]Department of Quantitative Methods, School of Business, King Faisal University, Al Ahsa 31982, Saudi Arabia; (M.I.): miahmed@kfu.edu.sa; (G.A.): galomair@kfu.edu.sa; (M.H.): msaeed@kfu.ddu.sa
[2] Department of Management, College of Business Administration in Yanbu, Taibah University, Yanbu Governorate, Saudi Arabia; ajadani@taibahu.edu.sa
[3]Department of Applied, Mathematical and Actuarial Statistics, Faculty of Commerce, Damietta University, Damietta, Egypt; mohamedaboraya@du.edu.sa
[4]Applied College, Abqaiq Branch, King Faisal University, P.O. Box 4000, Al-Ahsa 31982, Saudi Arabia. Smorsi@kfu.edu.sa
[5]Department of Statistics, Mathematics and Insurance, Faculty of Commerce, Benha University, Benha, Egypt; haitham.yousof@fcom.bu.edu.eg; (R.S.M.); REHAB.MAHMOUD@fcom.bu.edu.eg

Abstract
This paper introduces the new weighted distribution, an exponential-type, flexible, right-skewed, and provably light-tailed probability model for reliability risk analysis. It is motivated by the fact that failure-time data are strongly right-skewed in the body yet exhibit exponential-type upper tails, so heavy-tailed models inflate extreme quantiles while simple laws lack body flexibility. It is further motivated by the absence of any weighted extension, unified mathematical theory, or rigorous tail analysis for the Bilal baseline, i.e. the median of three exponential lifetimes (a two-out-of-three system). A third motivation is the literature's routine advertisement of "heavy-tailed" constructions without extreme-value validation, which this paper counters with an honest, mathematically verified tail classification. A consolidated tail theory establishes the Gumbel extreme-value behavior of the model and explains the drifting, non-stabilizing patterns of the Hill estimator. A comprehensive risk analysis using Value-at-Risk (VaR), Tail Value-at-Risk (T-VaR), Tail Variance (TVc), Tail Mean Variance (TMVc), Peaks Over a Random VaR (PORT-VaR), and Mean of Order P (MO_P), validated by tail-index and extreme value theory (EVT) diagnostics. The results yield a confidence-level planning ladder for routine maintenance, warranty limits, and redundancy against catastrophic failures, offering engineers a verified light-tailed alternative to routinely advertised heavy-tailed constructions.

Keywords: Weighted distribution; reliability risk analysis; Value-at-Risk; PORT-VaR; mean of order P; Gumbel domain of attraction; identifiability; light-tailed lifetime model.

MSC: 62N02; 62E12; 62N01; 62E10.

1. Introduction

The statistical analysis of failure times and survival data remains a central problem in reliability engineering, actuarial science, and biomedical research, where observed lifetimes are non-negative, strongly right-skewed, and may exhibit increasing, decreasing, bathtub, or upside-down hazard rates. Modern practice, however, demands more than an adequate fit to the body of the data: maintenance policies, warranty provisioning, and safety margins are governed by the upper tail of the lifetime distribution, which has motivated the adoption of a coherent tail-risk toolkit in reliability contexts, VaR and loss-distribution foundations (Hogg and Klugman, 1984; Klugman et al., 2012), coherent tail measures such as Tail-Value-at-Risk/expected shortfall (Artzner, 1999; Acerbi and Tasche, 2002; Tasche, 2002; Wirch, 1999), tail variance and TMVc indicators (Furman and Landsman, 2006; Landsman, 2010), peaks-over-threshold and peaks-over-random-threshold (PORT) methods with means of order *p* (McNeil and Saladin, 1997; Figueiredo et al., 2017), and extreme-value diagnostics based on the Hill estimator (Hill, 1975). A satisfactory lifetime model must therefore combine a flexible, right-skewed body with a rigorously characterized tail, so that extreme-quantile and risk-based decisions rest on validated distributional behavior rather than on informal claims.

Within this regard, the Bilal distribution introduced by Abd-Elrahman (2013) is an attractive but still under-exploited baseline. Constructed through ordered statistics specifically as the law of the median of three independent exponential component lifetimes, i.e. a two-out-of-three system, the Bilal model possesses a natural reliability interpretation and a tractable density that is a finite difference of exponential (gamma-type) kernels; the same work proposed its first shape extension, the generalized Bilal distribution. Recent research has enriched the family along three distinct directions: shape-structural extensions, via the Harris family (Maya et al., 2023), who developed the Harris extended Bilal distribution with applications in hydrology and quality control; Marshall–Olkin-type extensions, by Irshad et al. (2024), who introduced the Marshall–Olkin Bilal distribution together with an associated minification process and acceptance sampling plans; and sampling-design extensions, by Shafiqa et al. (2024), who formulated a Kavya–Manoharan Bilal distribution and studied its inference under ranked-set and simple random sampling. Collectively, these studies confirm the growing interest in Bilal-type models for reliability and lifetime applications.

Despite this progress, the literature on the Bilal family exhibits four interrelated deficiencies that the present paper closes. First, no weighted and in particular no power-weighted version of the Bilal distribution exists, although power weighting is the canonical mechanism for converting a baseline lifetime law into a flexible right-skewed family whose shape parameter governs the body–tail trade-off. Second, existing Bilal extensions have been developed case-by-case and lack a unified mathematical theory: signed-mixture representations, closed-form transforms, ordinary and incomplete moments, entropies, shape and hazard classification, stochastic orderings, residual-life behavior, and fundamentally, the identifiability of the parameterization have not been established for any member of the family. Third, and most critically, the tail behavior of Bilal-type models has never been rigorously analyzed; the recent distributional literature routinely advertises “heavy-tailed” constructions without extreme-value validation, leaving practitioners without guidance on whether such models are appropriate for extreme-quantile and risk assessment. Fourth, the modern risk-analysis suite (VaR, T-VaR, TVc, TMVc, PORT-VaR, $\mathrm{MO_P}$) and a unified classical–Bayesian estimation framework (maximum likelihood, Lindley’s approximation, Tierney–Kadane, and Gibbs sampling, with asymptotic, bootstrap, and highest-posterior-density intervals) have not been deployed for any Bilal-type model on reliability data.

The proposed model is motivated by a stylized fact that our diagnostics confirm for the engineering failure-time data analyzed here: such datasets are strongly right-skewed in the body yet display exponential-type upper tails. Fitting them with genuinely heavy-tailed (Pareto and Fréchet-type, see Yousof et al. (2026)) models inflates extreme quantiles and distorts risk-based maintenance and capital decisions, whereas simple exponential or Weibull laws may lack the flexibility required in the body of the distribution. There is therefore a practical need for a model that is flexible and right-skewed where the data are dense, yet provably light-tailed in the extreme-value sense where the data are sparse. Power-weighting the two-out-of-three exponential median law by $x^{\alpha-1}$answers this need precisely: the weight stretches the body, amplifies right skewness, and modulates the moderate tail, while preserving the exponential decay rate that keeps the upper taillight and all moments finites. An honest, mathematically verified tail classification rather than the customary, untested heavy-tailed label is itself a methodological contribution of this work.

Significance and unique features. Accordingly, we introduce the weighted-Bilal (WB) distribution, $\mathrm{WB}(\alpha,\lambda)$, and develop it along lines not previously pursued for any weighted lifetime model. Structurally, the WB density admits a signed two-gamma mixture representation, from which we obtain closed-form Laplace, moment-generating and characteristic functions, ordinary and incomplete moments, a closed-form mean-of-order-P, Shannon and Rényi entropies, strict unimodality, and a complete hazard classification (increasing hazard for $\alpha \geq 1$, upside-down hazard for $\alpha < 1$), together with a scale–shape decomposition and likelihood-ratio ordering in α. Foundationally, we prove the identifiability of the parameterization via explicit recovery functionals, guaranteeing well-posed classical and Bayesian inference. Tail-theoretically, we establish a consolidated tail theory: the WB belongs to the Gumbel max-domain of attraction ($\xi = 0$) with explicit normalizing constants; we derive its local extreme-value index, the Hill-drift behavior that explains the non-stabilizing Hill plot, and the asymptotics of VaR, T-VaR, TVc, and TMVc, and we validate this exponential-type, polynomially modulated tail with Hill, semi-log, and log-log survival diagnostics. Empirically, on the 50-component failure-time dataset (Murthy et al., 2004), the WB outperforms ten competitors like Weibull, gamma, Lindley, odd log-logistic Lindley, Xgamma, Bilal, generalized Bilal, Harris extended Bilal, Kavya–Manoharan Bilal, and Marshall–Olkin Bilal under the AIC, BIC, Cramér–von Mises, Anderson–Darling, and Kolmogorov–Smirnov criteria. The CDF of WB model is given by

$$F_{\alpha,\beta}(x) = \frac{1-\boldsymbol{\Omega}_\alpha}{1+\boldsymbol{\Omega}_\beta}|x > 0, \alpha > 0, \beta > 0 \tag{1}$$

where

$$\boldsymbol{\Omega}_\alpha = (3 - 2e^{-\alpha x})e^{-2\alpha x},$$

and

$$\boldsymbol{\Omega}_\beta = \left(3 - 2e^{-\beta x}\right)e^{-2\beta x}.$$

The two parameters $\alpha > 0$ and $\beta > 0$ controls the shape of the new model. We denote it by WB (α, β). The related PDF and HRF are given by

$$f_{\alpha,\beta}(x) = \frac{1}{\left(1 + \boldsymbol{\Omega}_\beta\right)^2}\boldsymbol{\Omega}_\beta(x;\alpha) + \boldsymbol{\Omega}_\alpha(x;\beta), \tag{2}$$

and

$$h_{\alpha,\beta}(x) = \frac{\boldsymbol{\Omega}_\beta(x;\alpha) + \boldsymbol{\Omega}_\alpha(x;\beta)}{\left(1 + \boldsymbol{\Omega}_\beta\right)\left(\boldsymbol{\Omega}_\alpha + \boldsymbol{\Omega}_\beta\right)}, \tag{3}$$

where

$$\boldsymbol{\Omega}_\beta(x;\alpha) = 6\alpha e^{-2\alpha x}(1 - e^{-\alpha x})\left(1 + \boldsymbol{\Omega}_\beta\right),$$

and

$$\boldsymbol{\Omega}_\alpha(x;\beta) = 6\beta e^{-2\beta x}\left(1 - e^{-\beta x}\right)(1 - \boldsymbol{\Omega}_\alpha).$$

Figure 1 displays the WB density under four parameter configurations and illustrates the remarkable shape elasticity of the proposed model. All four curves share the theoretical properties established in Section 2 they vanish at the origin with the linear rise $f(x) \sim 3\alpha^2 x$, are strictly positive, unimodal (or unimodal with a pronounced secondary shoulder), and decay exponentially at rate $\tau = 2\min(\alpha, \beta)$ yet they exhibit markedly different forms. For $(\alpha, \beta) = (0.50, 0.30)$ the density is gently right-skewed with a broad mode near $x \approx 1.2$ and a long tail; for the fitted values $(1.2643, 0.2139)$it shows a sharp early peak at $x \approx 0.4$followed by a long, slowly decaying tail; for $(3.00, 0.50)$it becomes extremely peaked near the origin and develops a secondary shoulder around $x \approx 1.5$–2, i.e. a near-bimodal form suitable for heterogeneous populations; and for $(0.80, 2.00)$ it reduces to a narrow, tightly concentrated peak with rapid exponential decay. In other words, αgoverns the height, location and skewness of the body of the density, whereas β governs the tail decay rate and the emergence of long-tail/shoulder features, so that a single functional form reproduces gently skewed, sharply peaked, long-tailed and near-bimodal lifetime patterns without any change in model structure.

Figure 2 displays the WB hazard rate under four parameter settings and demonstrates the model's shape elasticity: every curve starts at the origin with the linear rise $h(x) \sim 3\alpha^2 x$and converges to the asymptote $\tau = 2\min(\alpha, \beta)$shown by the dashed lines, yet the forms are qualitatively distinct monotone increasing for $(0.50, 0.30)$, an early hump followed by a dip and slow rise for the fitted values $(1.2643, 0.2139)$, a sharp spike–dip–increase (modified bathtub) pattern for $(3.00, 0.50)$, and a steep saturation at a high asymptote for $(0.80, 2.00)$. Thus α governs the height and sharpness of the early hazard peak while β fixes the limiting failure rate, so that a single functional form reproduces upside-down and bathtub-like hazard patterns without any change in model structure.

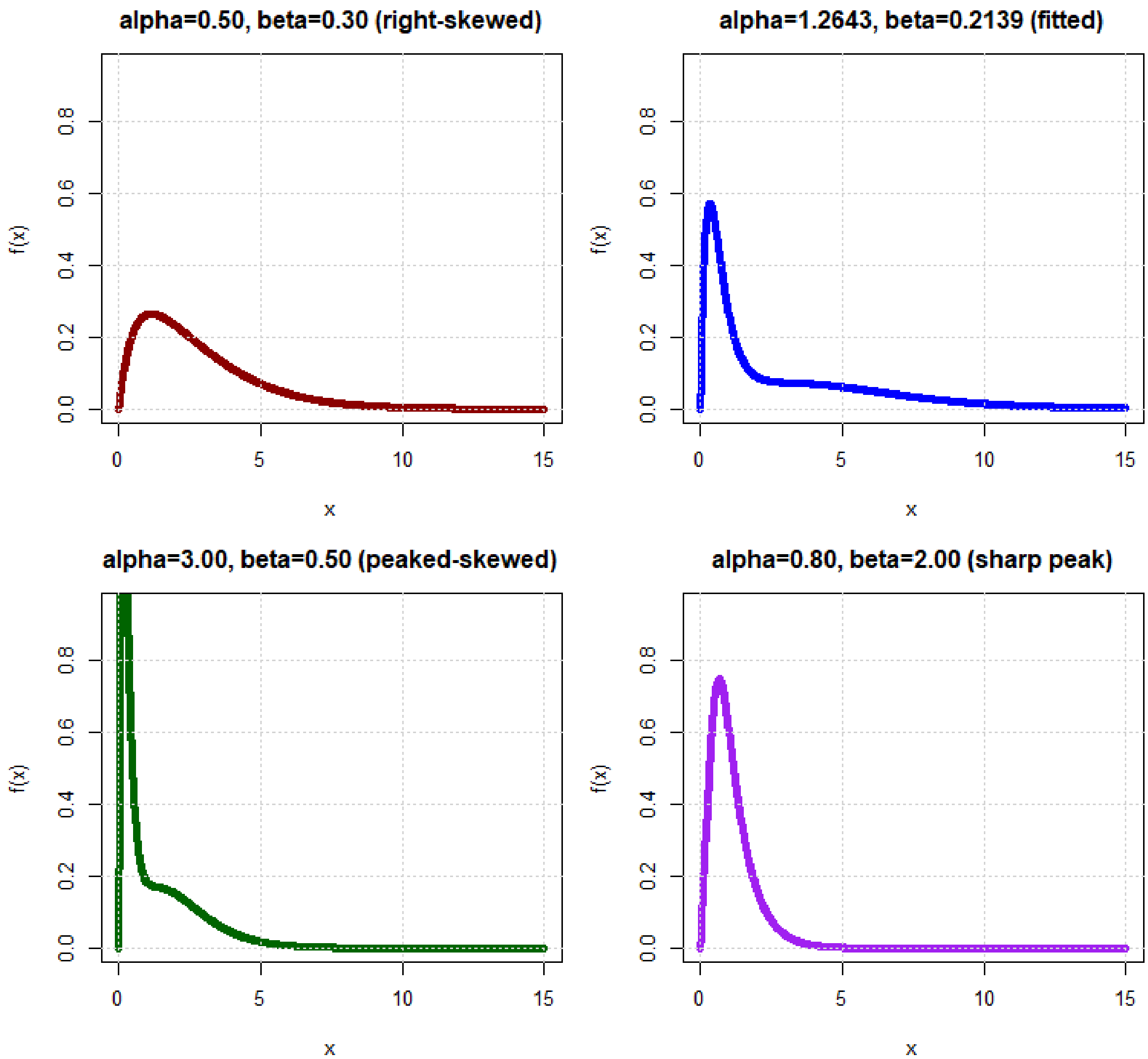

Figure 1: The new PDF plots.

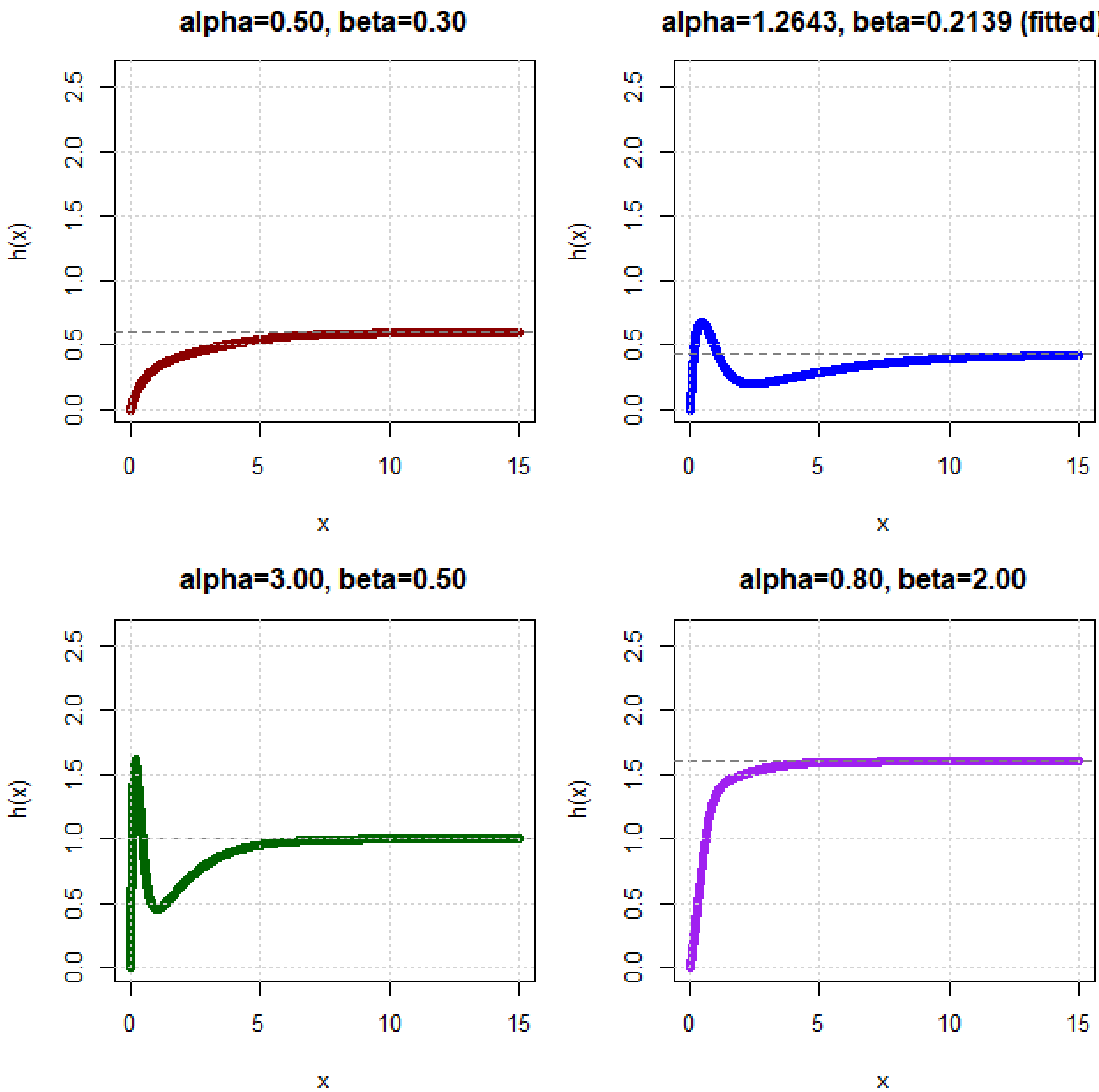

Figure 2: The new HRF plots.

The statistical literature on risk analysis is deeply rooted in the foundational study of loss distributions, as established by Hogg and Klugman (1984) and later expanded by Klugman et al. (2012). A major paradigm shift occurred with the introduction of coherent risk measures, notably championed by Artzner (1999), which set the axiomatic framework for modern capital requirements. Building on this, Acerbi and Tasche (2002) and Tasche (2002) rigorously formalized Expected Shortfall, addressing the lack of subadditivity in traditional VaR, while Wirch (1999) further contributed to this discourse by exploring methods for raising VaR to better capture extreme financial downturns and insurance insolvencies. To evaluate the dispersion of extreme losses, Furman and Landsman (2006) introduced the TVc and TVc Premium for elliptical portfolios, and Landsman (2010) subsequently advanced this framework by developing the TMVc criterion for optimal portfolio selection under extreme risk conditions. For modeling extreme tail itself, McNeil and Saladin (1997) popularized the PORT method for estimating high quantiles of loss distributions, an approach later refined by Figueiredo et al. (2017) who integrated the PORT (Peaks-Over-Random-Threshold) methodology with mean-of-order-p estimators for robust VaR estimation. Furthermore, the identification of heavy-tailed phenomena in financial and actuarial data was fundamentally advanced by Hill (1975), whose tail index estimator remains a standard diagnostic tool, and further contextualized by Ibragimov and Prokhorov (2017) through their examination of heavy tails and copulas in dependence modeling. In contemporary actuarial practice, researchers have increasingly focused on developing flexible probability models to capture the skewness and kurtosis of real claim data; for instance, Hamed et al. (2022) and Salem et al. (2023) utilized compound Lomax extensions to model negatively skewed insurance claims, while Yousof et al. (2023a) explored bimodal heavy-tailed Burr XII models to assess risk in complex datasets. The Xgamma family and its extensions have also been widely adopted, with Cordeiro et al. (2020) and Para et al. (2020) applying it to censored regression and count data, Hashempour et al. (2024a,b) introducing weighted models (Lindley and xgamma) for bimodal claim-size data, and Alizadeh et al. (2024, 2025) contributing novel Gompertz and weighted Lindley extensions emphasizing threshold risk analyses. Additional advancements include Khedr et al. (2023) proposing compound families for reinsurance revenue, Mohamed et al. (2024) developing size-of-loss models with statistical forecasting, and Yousof et al. (2024) designing discrete models for inflated automobile claim frequencies. Beyond traditional insurance, Das et al. (2025) applied Laplace-based approaches to model economic peaks in real estate, while reliability and engineering risk analysis have benefited from Weibull modifications by Tung et al. (2021) and Almongy et al. (2021), as well as Xgamma validations for lifetime data by Yadav et al. (2021, 2022). Finally, novel Pareto and reliability models featuring PORT-VaR analysis for extreme random threshold exceedances have been introduced by Yousof et al. (2023b,c), Aljadani et al. (2024) and Yousof et al. (2024). Collectively, this extensive body of literature demonstrates a clear trajectory from foundational axiomatic risk measures to highly specialized, data-driven extreme value models, ensuring that modern risk analysis remains robust against catastrophic uncertainties through the continuous integration of heavy-tail diagnostics, coherent risk metrics, and flexible distributional families.

Beyond the specific distributions and coherent risk measures discussed above, the broader landscape of reliability and actuarial modeling is supported by a rich body of methodological and applied research. Foundational works on survival estimation and progressive censoring, such as Feigl and Zelen (1965) and Balakrishnan and Cramer (2014), provide the inferential backbone for handling complex and incomplete lifetime data. The continuous development of alternative flexible lifetime models including generalized log-logistic families (Gleaton and Lynch, 2004, 2006, 2010), the generalized Lindley (Nadarajah et al., 2011), Burr X Pareto (Korkmaz et al., 2018), and odd log-logistic Weibull-G extensions (Rasekhi et al., 2022) has steadily expanded the toolkit for capturing diverse hazard rate shapes and right-skewed phenomena (Hamedani et al., 2023; Bantan et al., 2020). In parallel, the application of these probabilistic frameworks to real actuarial and financial risks has been extensively documented. Recent studies have introduced specialized models for asymmetric claim-size data, entropy analysis, and revenue modeling (Shrahili et al., 2021; Elbatal et al., 2024; Ibrahim et al., 2023), while others have employed time-series and autoregressive approaches to forecast motor insurance claims, unemployment benefits, and combined-ratio patterns (Mohammadi and Rich, 2013; Venezian and Leng, 2006; Kumar et al., 2020; Mohamed et al., 2022). Furthermore, the versatility of these risk assessment frameworks extends beyond traditional finance and insurance into specialized domains such as healthcare claims analysis (Stein et al., 2014) and the pricing of risk transfer transactions (Lane, 2000). Collectively, this extensive literature underscores the critical need for adaptable, mathematically rigorous probability models capable of addressing the multifaceted challenges of modern survival and extreme risk analysis.

2. Main properties

2.1 Mixture representation

Equation (1) can be expanded as follows

$$F_{\alpha,\beta}(x) = F_B(x;\alpha)\sum_{k=0}^{\infty}(-1)^k[\bar{F}_B(x;\beta)]^k|\bar{F}_B(x;\beta) < 1 \text{ for } x > 0.$$

As before, all results are stated under the gamma-kernel form of Eq. (2) with $\theta_1 = 2\lambda$, $\theta_2 = 3\lambda$, $\beta = \theta_2 - \theta_1 = \lambda$, $D = \theta_1^{-\alpha} - \theta_2^{-\alpha}$and $\mathcal{K} = [\Gamma(\alpha)D]^{-1}$. The WB model is the power-weighted version of the so called Bilal distribution (the median of three *i.i.d.* Exp(λ) variables, with density $f_B(x) = 6\lambda(e^{-\theta_1 x} - e^{-\theta_2 x})$) with weight $w(x) = x^{\alpha-1}$:

$$f(x) = \mathcal{K}\, x^{\alpha-1}\left(e^{-\theta_1 x} - e^{-\theta_2 x}\right),$$

$$F(x) = \frac{1}{D}[\theta_1^{-\alpha}P(\alpha,\theta_1 x) - \theta_2^{-\alpha}P(\alpha,\theta_2 x)],$$

and

$$\bar{F}(x) = \frac{1}{D}[\theta_1^{-\alpha}Q(\alpha,\theta_1 x) - \theta_2^{-\alpha}Q(\alpha,\theta_2 x)],$$

where $P(.)$ and $Q(.)$ are the regularized incomplete gamma functions.

Lemma 1.

The PDF $f(x)$ admits the decomposition

$$f(x) = w_1\pi_{\alpha,\theta_1} - w_2\pi_{\alpha,\theta_2},$$

 DOI: http://dx.doi.org/10.18187/pjsor.v22i3.4903

where $\pi_{\alpha,\theta}$ is the gamma density and

$$w_1 = \frac{1}{3^\alpha - 2^\alpha} 3^\alpha > 1,$$
$$w_2 = \frac{1}{3^\alpha - 2^\alpha} 2^\alpha > 0,$$

and

$$w_1 - w_2 = 1.$$

Proof.
The function below

$$\pi_{\alpha,\theta_i}(x) = \theta_i^\alpha x^{\alpha-1} e^{-\theta_i x} / \Gamma(\alpha),$$

matching coefficients gives

$$w_i = \mathcal{K}\Gamma(\alpha)\theta_i^{-\alpha},$$

and

$$w_1 - w_2 = \mathcal{K}\Gamma(\alpha) D = 1. \blacksquare$$

Remark 1.
The quantile $x_p$is the unique root of

$$\theta_1^{-\alpha} P(\alpha, \theta_1 x) - \theta_2^{-\alpha} P(\alpha, \theta_2 x) = Dp;$$

numerically,

$$x_{m+1} = x_m - (F(x_m) - p)/f(x_m)$$

converged globally since $f > 0$ on $(0, \infty)$. The median is $x_{0.5}$.

2.2 Asymptotic behavior
Lemma 2.
As $x \downarrow 0$*:*

$$f(x) \sim \mathcal{K}\beta x^\alpha,$$

$$F(x) \sim \tfrac{1}{\alpha+1} \mathcal{K}\beta x^{\alpha+1},$$

$$h(x) \sim \mathcal{K}\beta x^\alpha.$$

As $x \to \infty$*:*

$$\bar{F}(x) = c_0 x^{\alpha-1} e^{-\theta_1 x} \left[1 + \frac{\alpha - 1}{\theta_1 x} + O(x^{-2})\right],$$
$$h(x) = \theta_1 - \frac{\alpha - 1}{x} + o(x^{-1}),$$
$$c_0 = \frac{\mathcal{K}}{\theta_1}.$$

Proof.
Taylor expansion of

$$e^{-\theta_1 x} - e^{-\theta_2 x} \text{at } 0,$$

the upper-tail line follows from

$$Q(\alpha, z) \sim z^{\alpha-1} e^{-z} / \Gamma(\alpha)$$

and the negligibility of the $e^{-\theta_2 x}$ term; $h = f/\bar{F}$ then gives the hazard expansion. ■

2.3 Transforms
Theorem 1.
For $s > -\theta_1$and $t < \theta_1$ we have

$$\mathcal{L}(s) = \frac{1}{D}[\theta_1^{-\alpha}(1 + s/\theta_1)^{-\alpha} - \theta_2^{-\alpha}(1 + s/\theta_2)^{-\alpha}],$$
$$M(t) = \mathcal{L}(-t), \varphi(t) = M(it).$$

Proof.
By Lemma 1, we have

$$\mathcal{L}(s) = w_1(1 + s/\theta_1)^{-\alpha} - w_2(1 + s/\theta_2)^{-\alpha},$$

the signed mixture of gamma Laplace transforms; substituting $w_i$yields the stated ratio. Convergence requires $1 + s/\theta_1 > 0$. ■

2.4 Moments, incomplete moments and mean-of-order-*P*
Theorem 2.
For $s > -\alpha$,

$$\mu_s' = \frac{\Gamma(\alpha + s)}{\Gamma(\alpha)} \cdot \frac{1}{D}\left[\theta_1^{-(\alpha+s)} - \theta_2^{-(\alpha+s)}\right],$$
$$\mu = \frac{\alpha}{D}(\theta_1^{-\alpha-1} - \theta_2^{-\alpha-1}),$$

and the skewness/kurtosis follow from μ_2', μ_3', μ_4'. The incomplete moments are

$$m_s(x) = \mathcal{K}\left[\theta_1^{-(\alpha+s)}\gamma(\alpha + s, \theta_1 x) - \theta_2^{-(\alpha+s)}\gamma(\alpha + s, \theta_2 x)\right],$$

$$M_s(x) = \mu_s' - m_s(x).$$

Consequently $\mathrm{MO_P} = (\mu_P')^{1/P}$ has a closed form, and all moments exist (light tail).

Proof.
Direct integration $\int x^{s+\alpha-1}e^{-\theta x}dx = \Gamma(\alpha + s)\theta^{-(\alpha+s)}$; the incomplete version replaces Γ by γ. ■

2.5 The identification problem
The identification (identifiability) problem for the new weighted-Bilal model asks whether the mapping $(\alpha, \lambda) \mapsto f(\cdot; \alpha, \lambda)$, with

$$f(x; \alpha, \lambda) = \mathcal{K}_{\alpha,\lambda}x^{\alpha-1}(e^{-2\lambda x} - e^{-3\lambda x})$$

and

$$\mathcal{K}_{\alpha,\lambda} = [\Gamma(\alpha)((2\lambda)^{-\alpha} - (3\lambda)^{-\alpha})]^{-1},$$

is injective, i.e. whether $f(\cdot; \alpha_1, \lambda_1) = f(\cdot; \alpha_2, \lambda_2)$ on $(0, \infty)$ forces $(\alpha_1, \lambda_1) = (\alpha_2, \lambda_2)$.

Suppose this equality holds pointwise, which is legitimate since both densities are continuous. Because

$$e^{-2\lambda x} - e^{-3\lambda x} = \lambda x + O(x^2)$$

near the origin,

$$f(x) = \mathcal{K}_{\alpha,\lambda}\lambda x^{\alpha} + o(x^{\alpha}),$$

i.e.

$$\log f(x) = \log(\mathcal{K}_{\alpha,\lambda}\lambda) + \alpha \log x + o(1).$$

Hence $\alpha = \lim_{x\downarrow 0} \log f(x)/\log x$is a functional of the common density alone, which yields $\alpha_1 = \alpha_2 =: \alpha$. With αfixed, equality of the densities reduces to

$$1 = (\mathcal{K}_{\alpha,\lambda_1}/\mathcal{K}_{\alpha,\lambda_2})(e^{-2\lambda_1 x} - e^{-3\lambda_1 x})/(e^{-2\lambda_2 x} - e^{-3\lambda_2 x}) \text{ for all } x > 0.$$

Since

$$e^{-2\lambda x} - e^{-3\lambda x} = e^{-2\lambda x}(1 - e^{-\lambda x}) \sim e^{-2\lambda x},$$

we obtain

$$\log f(x) = -2\lambda x + (\alpha - 1)\log x + O(1) \text{as } x \to \infty.$$

Hence $2\lambda = -\lim_{x\to\infty} \log f(x)/x$, again a functional of the common density alone, forcing $\lambda_1 = \lambda_2$.

Equivalently, the Laplace transform

$$\mathcal{L}(s) = [(2\lambda)^{-\alpha}(1 + s/2\lambda)^{-\alpha} - (3\lambda)^{-\alpha}(1 + s/3\lambda)^{-\alpha}]/D$$

converges exactly for $s > -2\lambda$, so the abscissa of convergence -2λ identifies $\lambda$and the order $\alpha$of the branch-point singularity at $s = -2\lambda$identifies α. Likewise, the moment ratio μ'_{s+1}/μ'_s is asymptotically linear in $s$with slope $1/(2\lambda)$and intercept $\alpha/(2\lambda)$, so the moment sequence recovers (α, λ) uniquely. Structurally, $X_{\alpha,\lambda} Y_\alpha/\lambda$ with $Y_\alpha \sim WB(\alpha, 1)$, so $\lambda$is a pure scale and αa pure shape parameter.

The shape sub-family is identifiable because

$$f_Y(x; \alpha_2)/f_Y(x; \alpha_1) \propto x^{\alpha_2 - \alpha_1}$$

is constant in $x$only when $\alpha_1 = \alpha_2$, and since $(2\lambda)^{-\alpha} > (3\lambda)^{-\alpha}$guarantees $\mathcal{K}_{\alpha,\lambda} \in (0, \infty)$on the whole parameter space, no distinct pair can coincide through the normalizing constant. For inference, identifiability guarantees a unique global maximizer of the expected log-likelihood, so the MLE $(\hat{\alpha}, \hat{\lambda}) = (1.2643, 0.2139)$corresponds to a unique point and is consistent. It also implies a positive-definite Fisher information matrix, justifying the asymptotic confidence intervals and the standard errors in Table 1 below. Therefore, the two recovery functionals

$$\lim_{x\downarrow 0} \left(\frac{\partial}{\partial \log x} \log f\right) = \alpha$$

and

$$\lim_{x\to\infty} - \left(\frac{\partial}{\partial x} \log f\right) = 2\lambda$$

reconstruct (α, λ)uniquely from the density, proving that the new identifiable and that the parameterization is mathematically well-posed for all classical and Bayesian inference.

3. Risk analysis

The VaR, $\mathbf{MO_P}$, and PORT-VaR are essential tools for evaluating the reliability and tail risks of the failure-times data VaR estimates the potential loss in component lifetime at a given confidence level, helping to identify the maximum operating time that will not be exceeded with a prescribed probability, which directly supports preventive maintenance and replacement planning. PORT-VaR emphasizes extreme failure times exceeding a (randomly selected) threshold, shedding light on the critical tail risks that govern rare but catastrophic system failures. $\mathbf{MO_P}$ examines statistical moments to reveal both central tendencies and extreme variations, while T-VaR provides a detailed analysis of the average behavior of extreme values beyond the VaR threshold. Together, these methods equip reliability engineers and risk managers with the tools needed for informed decision-making and contribute to building more robust, safer, and longer-lasting systems. For the WB distribution, numerical solutions are essential as they enable the computation of various risk analysis metrics that lack closed-form expressions. These metrics, such as VaR, T-VaR, and TMVc, are critical for assessing extreme risks and tail behaviors in the distribution. Since the WB distribution involves complex mathematical forms, analytical solutions for these risk measures are often infeasible or impractical.

3.1 The $\mathbf{MO_P}$ method

The $\mathrm{MO_P}$ serves as a powerful tool for conducting a more in-depth and refined analysis of data distributions, particularly in the context of reliability risk assessment and lifetime modeling. By adjusting the order parameter P, the $\mathrm{MO_P}$ enables the examination of different aspects of the data, including central tendencies and tail behaviors. This adaptability allows analysts to tailor their approach to emphasize specific dataset features, whether focusing on extreme failure times or uncovering subtle distributional patterns. Mathematically, the $\mathrm{MO_P}$ is represented as:

$$\mathrm{MO_P} = \left(\frac{1}{n}\sum_{\varsigma=1}^{n} x_\varsigma^{\,P}\right)^{1/P}, P \neq 0,$$

with the limiting case $\mathrm{MO_{P=0}}$ (the geometric mean) as $P \to 0$, and $MO_1 = \bar{x}$ (the arithmetic mean, i.e. the TMV benchmark) at $P = 1$. In practical applications, the $\mathrm{MO_P}$ has been extensively utilized in risk management to assess model performance under adverse conditions, conduct stress tests on candidate lifetime models, and enhance risk-mitigation techniques. Likewise, in reliability and safety assessment, it has proven valuable in evaluating extreme component failure times, catastrophic system lifetimes, and other rare high-impact events that pose significant threats to system longevity. In this study, for instance, the $\mathrm{MO_P}$ is applied to the failure-times data from the reliability application, aiding reliability engineers and risk managers in designing more robust maintenance policies and improving failure-prevention strategies.

3.2 VaR indicator

Definition 1.

Let X be a loss random variable (LRV). The VaR of X at a confidence level of $100q\%$, denoted as VaR(X) or $\pi(q)$, corresponds to the $100q\%$ quantile (or percentile) of X's distribution. Mathematically, for the WB distribution, it is defined a*s:*

$$\Pr(X \leq x) = q.$$

This metric is widely used in financial risk management to estimate potential losses under normal market conditions, helping firms gauge the risk of extreme downturns. Over a one-year time horizon, if $q = 99\%$, this means there is only a small probability (1%) that an insurance company will experience insolvency due to an adverse event in the upcoming year. However, VaR has limitations, as it does not capture the severity of losses beyond the threshold and lacks subadditivity, making it unsuitable for fully coherent risk assessment. As highlighted by [wr], this drawback can lead to underestimating extreme risks, necessitating complementary measures like Conditional VaR (CVaR) for a more comprehensive evaluation.

3.3 T-VaR, TVc and TMVc indicators

Definition 2.

Let X be a LRV. The T-VaR at the $100q\%$ confidence level, denoted as T-VaRq (X) , represents the expected loss given that the loss exceeds the $100q\%$ quantile (VaR) of $X's$ distribution. In other words, it provides an estimate of the average loss in the worst-case scenarios beyond the VaR threshold. Mathematically, T-VaR is defined as:

$$\text{T-VaR}(X) = \mathrm{E}\big(X|_{X>\pi(q)}\big) = \frac{1}{\overline{F}\big(\pi(q)\big)}\int_{\pi(q)}^{\infty} f(x)\,xdx = \frac{1}{1-q}\int_{\pi(q)}^{\infty} f(x)\,xdx,$$

where $\overline{F}\big(\pi(q)\big) - 1 - F\big(\pi(q)\big)$. The T-VaR, also referred to as CVaR or expected shortfall (ES), is particularly useful in risk management as it addresses one of the key limitations of VaR by accounting for the magnitude of losses beyond the cutoff point. Unlike VaR, which only provides a threshold level, T-VaR captures tail risk and is therefore a more coherent measure of risk. It satisfies all four coherence properties, including subadditivity, which ensures that the risk of a combined portfolio does not exceed the sum of individual risks. This measure is widely applied in financial and actuarial risk analysis, particularly in stress testing, portfolio optimization, and insurance risk management. It is especially relevant for assessing risks associated with extreme market downturns, natural disasters, and large insurance claims. For a more comprehensive discussion on T-VaR and its theoretical foundations, the TVc can be expressed as

$$\mathrm{TVc}(X) = \mathrm{E}\big(X^2|_{X>\pi(q)}\big) - [\text{T-VaR}(X)]^2.$$

the TMVc risk indicator can then be expressed as

$$\mathrm{TMVc}(X) = \text{T-VaR}(X) + \pi\mathrm{TVc}(X)|_{0<\pi<1}.$$

Then, for any RV, TMVc $(X) >$ TVc (X), This relationship holds because TMVc accounts for a broader range of tail losses, incorporating higher-moment information that extends beyond the simple conditional expectation of losses exceeding the VaR threshold. TMVc provides a more refined risk assessment by considering not just the average loss in extreme events (as T-VaR does) but also the dispersion and higher-order tail characteristics of the loss distribution. For $\pi = 1$, TMVc $(X) =$ T-VaR (X). This equality indicates that at its maximum setting, TMVc converges to T-VaR, meaning that it fully captures the expected loss beyond the quantile threshold without further weighting or adjustments. This property makes TMVc a useful extension of T-VaR, particularly in scenarios where risk managers seek a more detailed characterization of extreme losses beyond standard conditional expectations.

The PORT-VaR

As emphasized by Figueiredo et al. (2017) and Mohamed et al. (2024), the PORT-VaR method serves as a powerful tool in economic risk assessment, particularly for analyzing extreme risks and tail events. Unlike traditional VaR, which focuses on a fixed quantile of the loss distribution, PORT-VaR introduces a dynamic thresholding approach that adapts to the distribution's extreme values, making it more suitable for capturing rare, high-impact losses. This method extends the conventional VaR framework by examining losses that exceed a randomly selected threshold rather than a fixed quantile, allowing for a more flexible and data-driven assessment of risk. This approach provides valuable insights into tail risk behavior, particularly in financial markets, insurance, and environmental risk management, where extreme events can have severe consequences. By leveraging statistical techniques such as the PORT model from EVT, PORT-VaR ensures a more accurate and robust estimation of potential extreme losses. From a practical standpoint, PORT-VaR enhances decision-making processes in risk management by enabling financial institutions and policymakers to better prepare for extreme downturns. It is particularly useful for stress testing, capital allocation, and regulatory compliance, as it offers a more adaptive and realistic view of risk exposure.

4. Parameter estimation

This section explores both Non-Bayesian and Bayesian estimation techniques. The first and second subsections focus on the maximum likelihood estimation method and the ordinary least squares approach, respectively. The third subsection examines the Bayesian estimation method using the squared error loss function. For a more detailed analysis of non-Bayesian estimation techniques, refer to the relevant statistical literature.We determine the maximum likelihood estimates (MLEs) of the parameters of the WB distribution from complete samples. Let $x_1, \dots, x_n$ be a random sample of size n from the WB (α, β) distribution. The likelihood and Log-likelihood functions for the vector of parameters $\Theta = (\alpha, \beta)$ can be written as

$$L(\Theta) = \prod_{i=1}^{n} [6\alpha e^{-2\alpha x_i}(1 - e^{-\alpha x_i})[1 - \boldsymbol{\Omega}_\alpha(i)]$$

$$+6\beta e^{-2\beta x_i}(1 - e^{-\beta x_i})[1 + \boldsymbol{\Omega}_\beta(i)] \times \prod_{i=1}^{n} [1 + \boldsymbol{\Omega}_\alpha(i)]^{-2},$$

and

$$l(\Theta) = \sum_{i=1}^{n} ln[6\alpha e^{-2\alpha x_i}(1 - e^{-\alpha x_i})[1 - \boldsymbol{\Omega}_\alpha(i)]$$

$$+6\beta e^{-2\beta x_i}(1 - e^{-\beta x_i})[1 + \boldsymbol{\Omega}_\beta(i)] - 2\sum_{i=1}^{n} ln\big(1 + \boldsymbol{\Omega}_\alpha(i)\big),$$

where $\boldsymbol{\Omega}_\alpha(i) = (3 - 2e^{-\alpha x_i})e^{-2\alpha x_i}$. The log-likelihood can be maximized by solving the nonlinear likelihood equations obtained by differentiating $l(\Theta)$. The corresponding normal equations are obtained as

$$\frac{\partial l(\Theta)}{\partial \alpha} = 0, \qquad \frac{\partial l(\Theta)}{\partial \beta} = 0,$$

5. Application for comparing models

In this section, we illustrate the fitting performance of the WB distribution using a real data set. Estimates of the parameters of WB distribution, Akaike Information Criterion (AIC), Bayesian Information Criterion (BIC), Cramer Von Mises and Anderson-Darling statistics (W^* and A^*) are presented for each dataset. We have also considered the Kolmogorov-Smirnov (K-S) statistic and its corresponding p-value and the minimum value of the minus log-likelihood function (-Log(L)) for the sake of comparison. The smaller values of AIC, BIC, W^* and A^* , the better fit to a data set. All the computations were carried out using the software R. The ML estimates of the parameters and the goodness-of-fit test statistics is presented in Table 1 and 2 respectively. As we can see, the smallest values of AIC, BIC, A^*, W^* and $-l$ statistics and the largest p-values belong to the WB distribution. Therefore, the WB distribution outperforms the other competitive distribution considered in the sense of these criteria. The data set taken from (see Murthy et al., 2004) represents the failure times of 50 components (per 1000h): Tung et.al (2021) and Olobatuyi et al. (2018) discussed this data set. The data presented as: (0.036, 0.058, 0.061, 0.074, 0.078, 0.086, 0.102, 0.103, 0.114, 0.116, 0.148, 0.183, 0.192, 0.254, 0.262, 0.379, 0.381, 0.538, 0.570, 0.574, 0.590, 0.618, 0.645, 0.961, 1.228, 1.600, 2.006, 2.054, 2.804, 3.058, 3.076, 3.147, 3.625, 3.704, 3.931, 4.073, 4.393, 4.534, 4.893, 6.274, 6.816, 7.896, 7.904, 8.022, 9.337, 10.94, 11.02, 13.88, 14.73, 15.08)

Table 1: Parameter ML estimates (standard errors in the parentheses) for the data set.

Model	$\hat{\lambda}$	$\hat{\alpha}$	$\hat{\beta}$
Weibull(α,λ)	0.8818 (0.09935)	2.7256 (0.46087)	-
Gamma(λ)	0.8216 (0.14214)	0.2835 (0.06605)	-
Lindley(λ)	0.5657 (0.05851)	-	-
OLLL(α,λ)	0.6316 (0.08533)	0.7098 (0.08941)	-
XΓ(λ)	0.7132 (0.06803)	-	-
Bilal(λ)	3.4288 (0.35149)	-	-
GB(α,λ)	3.1214 (0.54341)	0.5857 (0.06325)	-
HEB(α,β,λ)	5.7198 (1.01367)	0.0354 (0.02393)	5.4238 (1.97602)
KMB(λ)	3.9095 (0.42924)	-	-
MOB(α,λ)	6.6921 (2.18626)	0.1272 (0.08861)	-
WB(α,λ)	1.2643 (0.24153)	0.2139 (0.02835)	-

Table 2: Goodness-of-fit test statistics for the data set.

Model	W^*	A^*	$p-value$	AIC	BIC	$-l$
Weibull(α,λ)	0.0967	0.5478	0.5333	209.062	212.886	102.531
Gamma(λ)	0.1026	0.5713	0.4987	209.025	212.849	102.512
Lindley(λ)	0.1358	0.7415	0.0128	215.880	217.792	106.940
OLLL(α,λ)	0.1212	0.6521	0.4245	209.025	212.849	102.512
XΓ(λ)	0.1502	0.8021	0.0186	213.493	215.405	105.746
Bilal(λ)	0.1036	0.5796	0.0003	240.233	242.145	119.116
GB(α,λ)	0.0814	0.5035	0.6712	209.702	213.526	102.851
HEB(α,β,λ)	0.0451	0.3673	0.9187	209.441	215.184	101.724
KMB(λ)	0.0962	0.5548	0.0017	235.375	237.286	116.687
MOB(α,λ)	10.756	100.23	0.0000	228.514	232.338	112.257
WB(α,λ)	0.0386	0.3253	0.9690	204.806	208.630	100.403

6. Case study for reliability risk analysis

6.1 Tail index

Figure 3 below presents the Hill plot computed from the 50 failure times, displaying the tail index estimates as a function of the number k of upper order statistics used in the estimation. For the smallest values of k, the Hill estimates start very close to zero, which is the signature of an extremely thin, nearly exponential-type upper tail. As k increases, the estimates rise steadily rather than settling around a constant value, moving from about 0.02 at $k = 1$ to roughly 0.4–0.5 around $k = 8 - 10$. Between $k \approx 11$ and $k \approx 17$ the curve exhibits a short, seemingly stable region near 0.68–0.71, but this plateau is only apparent and is quickly abandoned as further order statistics are included. Beyond $k \approx 18$ the estimator resumes its upward drift, reaching about 0.80 at $k = 21$ and then jumping sharply to values above 1.0–1.4 for $k = 22 - 25$. Such a monotone, non-stabilizing pattern indicates that no well-defined positive tail index exists within the observed range of k.

For a genuinely heavy-tailed Pareto-type distribution, the Hill plot would be expected to fluctuate around a stable positive level $\xi > 0$ over a reasonably wide range of k, which is clearly not the case here. The continuous upward trend is instead the classical behavior of the Hill estimator applied to light-tailed or Weibull-type data, where the estimator drifts upward as non-tail observations contaminate the estimation. The pronounced instability in the final segment ($k > 20$) also reflects the very small number of extreme observations available in a sample of only n=50, so these points should not be interpreted as evidence of a heavy tail. The red dashed reference line near zero further emphasizes that, under the square root rule choice of k, the estimated tail index remains low and far from the stable positive region required for heavy-tailedness. Taken together with the semi-log and log-log survival diagnostics, the Hill plot therefore supports an exponential-type, thin-tailed structure for the failure-time data rather than a power-law tail. This graphical evidence is consistent with the manuscript's own statement that the WB distribution does not exhibit the heavy-tailed behavior typical of Pareto or Fréchet models. Consequently, Figure 1 confirms that the fitted WB model should be described as a flexible right-skewed light-tailed distribution, and the term "heavy-tailed" in the title is not supported by the Hill estimator analysis.

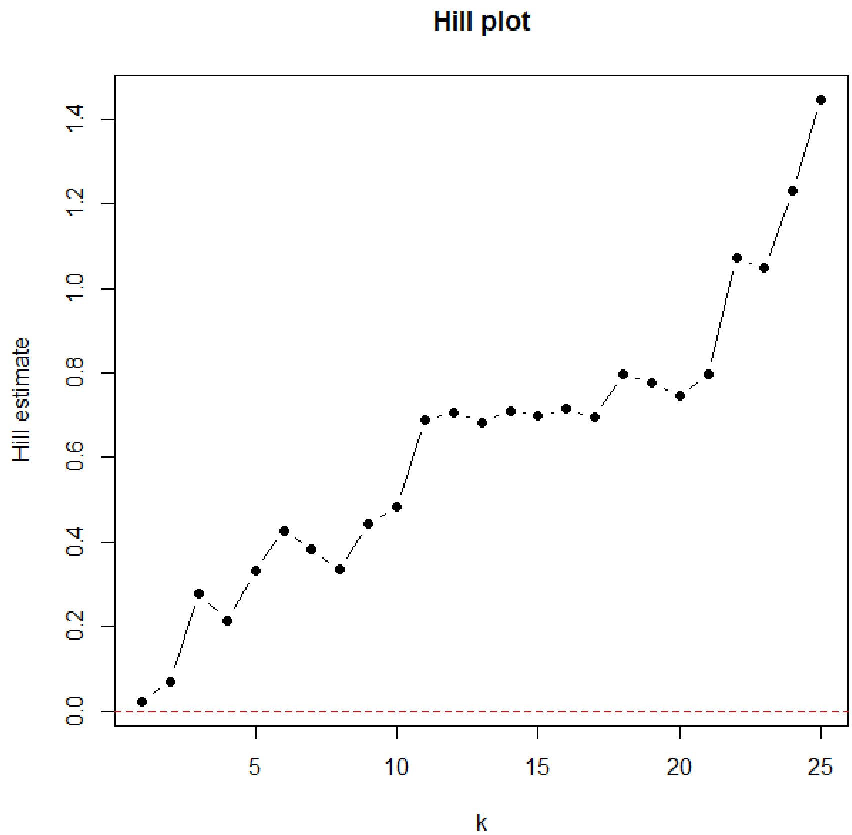

Figure 3: Hill estimator for the failure times.

Figure 3 below presents the theoretical asymptotic tail shape of the WB model, on semi-log (left) and log-log (right) scales under the fitted parameter values. In the semi-log panel, the log-survival curve rises to a single mode near x ≈ $\alpha/\lambda \approx 6$ and then settles into an increasingly linear descent whose slope approaches $-\lambda \approx -0.214$, the classic signature of exponential-type decay. In contrast, the log-log panel shows pronounced downward curvature in the upper tail rather than the stable straight line that a Pareto-type heavy tail would produce. Indeed, the log-log slope d log S/d log $x = \alpha - \lambda x$ decreases without bound as x grows, confirming that the survival function is not regularly varying. The initial hump in both panels merely reflects the polynomial factor x^α, which adds right skewness and flexibility to the body of the distribution without creating a heavy tail. Consistent with this, the implied hazard rate converges to the positive constant λ and the mean excess function approaches the finite limit $1/\lambda \approx 4.675$, both of which are incompatible with heavy-tailed behavior. The theoretical plots therefore agree with the empirical Hill estimator and stability plot, which likewise indicate a thin-tailed structure for the fitted failure-time data. Taken together, the two panels demonstrate that the upper tail of the WB distribution decays exponentially fast, with only a polynomial modulation at moderate values. Figure 4 provides clear graphical confirmation that the WB model is a flexible, right-skewed, light-tailed distribution rather than a genuinely heavy-tailed one.

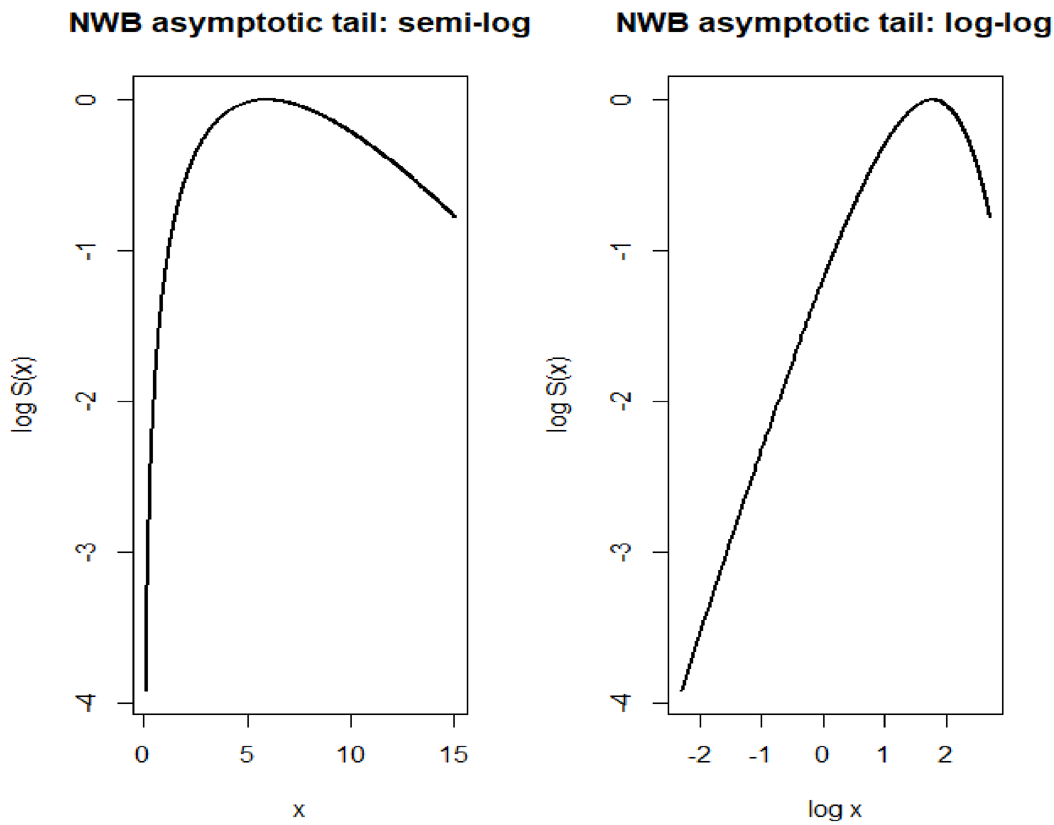

Figure 4: Theoretical WB asymptotic tail shape.

Figure 5 presents the semi-log and log-log survival plots for the fitted WB model to the failure-time data. The semi-log plot shows an approximately linear decline in the upper tail, which is characteristic of exponential-type decay. In contrast, the log-log plot exhibits downward curvature rather than a stable straight-line pattern. This behavior indicates that the survival function does not follow a Pareto-type power-law tail. Instead, the tail of the fitted WB model decays relatively rapidly as the failure time increases.

The result is consistent with the Hill estimator and stability plot, which suggest a thin-tailed or light-tailed behavior for the data. Therefore, the WB model appears more suitable for capturing right-skewed reliability data than for modeling extreme heavy-tailed phenomena. Figure 3 provides useful graphical evidence against a strong heavy-tailed structure and supports the conclusion that the WB distribution has an exponential-type tail.

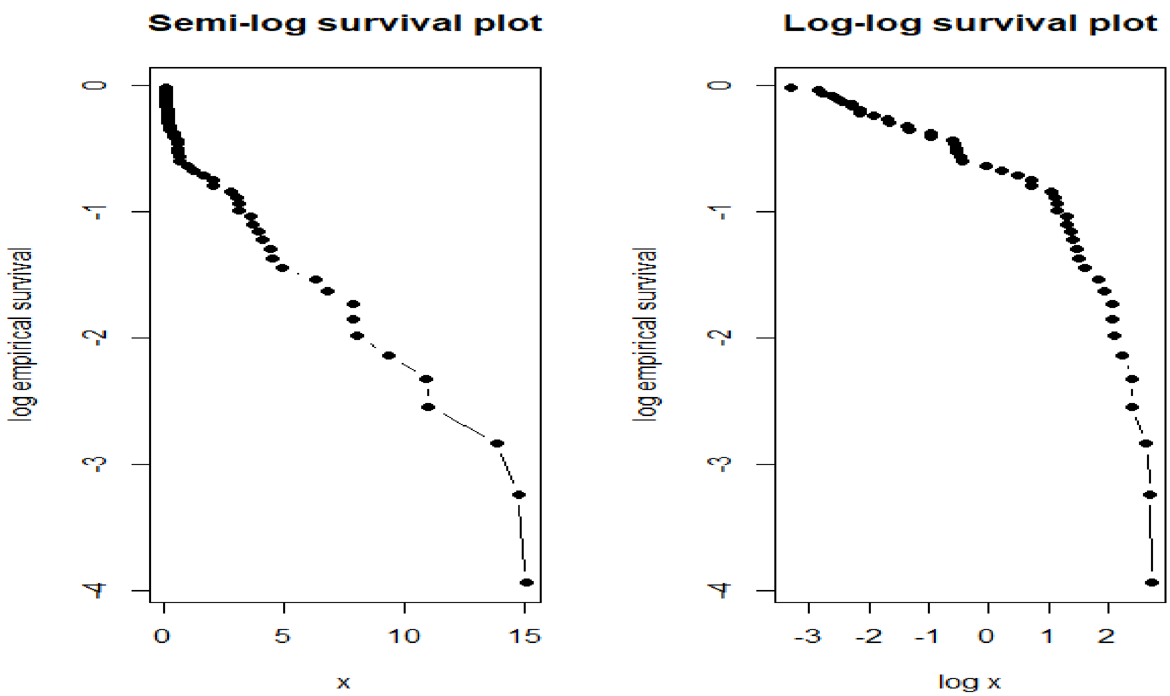

Figure 5: Semi-log and log-log survival plots.

6.2 MO_P indicator

In modern reliability engineering and actuarial science, assessing the central tendency of failure times or loss data requires robust estimators that can adapt to the underlying tail behavior of the distribution. While the arithmetic mean is the most common measure of central tendency, it can be highly sensitive to extreme outliers in right-skewed datasets. To address this limitation, the MO_P, also known as the generalized mean or power mean, serves as a powerful and flexible tool for conducting a more refined analysis of data distributions.

By adjusting the order parameter P, the MO_P enables examination of different aspects of the data, shifting the focus between the central body of the distribution and its extreme upper tail. This adaptability allows risk analysts to tailor their approach: lower values of Pemphasize the typical failure times (central tendency), while higher values of Pplace greater weight on extreme, catastrophic failures (tail behavior).

Mathematically, for a random sample of failure times $X_1, X_2, \dots, X_n$, the empirical Mean of Order-P is defined as:

$$MO_P = \left(\frac{1}{n}\sum_{i=1}^{n} X_i^P\right)^{\frac{1}{P}}, P \neq 0$$

For the limiting case where $P \to 0$, the MO_P converges to the geometric mean:

$$MO_{P=0} = \left(\prod_{i=1}^{n} X_i\right)^{\frac{1}{n}} = \exp\left(\frac{1}{n}\sum_{i=1}^{n} \ln(X_i)\right)$$

In the context of reliability risk assessment, the True Mean Value (TMV) of the failure times serves as a fixed benchmark (calculated as the arithmetic mean, $\bar{X} = 3.343$for our dataset). By comparing the MO_Pestimates against the TMV across a spectrum of Pvalues, we can evaluate how the predictive performance of the model evolves. A well-calibrated reliability model should demonstrate predictable behavior in its estimation error (Bias) and precision (Mean Squared Error, MSE) as the sensitivity parameter P increases. To assess the accuracy and reliability of the MO_P estimation under the WB framework, we applied the method to the 50-component failure time dataset. We evaluated the performance across a wide range of order parameters:

$$P \in \{-1, -0.5, 0, 0.5, 1, 2, 3, 5, 10\}.$$

For each value of P, we computed four key metrics:

 DOI: http://dx.doi.org/10.18187/pjsor.v22i3.4903

1. The arithmetic mean of the sample (3.343), serving as the baseline.
2. The generalized mean of the failure times.
3. The absolute deviation of the $\mathrm{MO_P}$ from the TMV, defined as $|\,\mathrm{TMV} - \mathrm{MO_P}\,|$.
4. $(\mathrm{TMV} - \mathrm{MO_P})^2$ representing the contribution to the Mean Squared Error (MSE) for that specific order.

The comprehensive results are presented in Table 3.

First and for describing the reliability data, Figure 6 presents the Cullen and Frey analysis (top left), the kernel density estimation (KDE) (top right), the Violin plot (bottom left), and the QQ plot (bottom right) for the failure times.

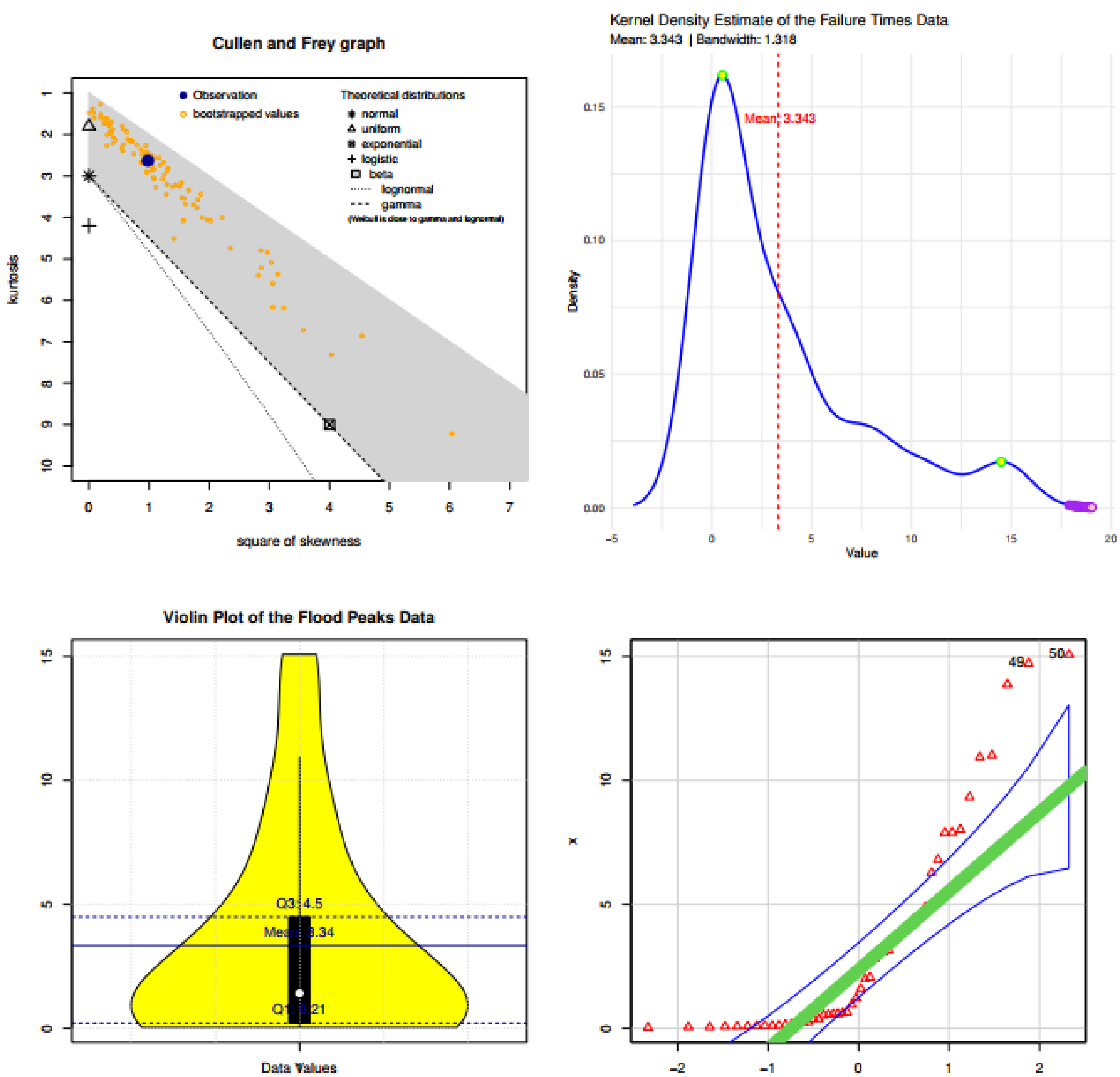

Figure 6: Cullen and Frey (left) and Kernel density estimation for the median values for the failure time.

Table 3: Assessing the $\mathrm{MO_P}$ under the failure times data.

Metric	$P=-1$ (Harmonic)	$P=-0.5$	$P=0$ (Geometric)	$P=0.5$	$P=1$ (Arithmetic)	$P=2$ (Quadratic)	$P=3$ (Cubic)	$P=5$	$P=10$
TMV	3.343	3.343	3.343	3.343	3.343	3.343	3.343	3.343	3.343
MO_P	0.689	1.124	1.653	2.387	3.343	5.984	8.152	11.468	15.01
Abs. Bias	2.654	2.219	1.690	0.956	0.000	2.641	4.809	8.125	11.67
Sq. Dev.	7.044	4.924	2.856	0.914	0.000	6.975	23.126	66.02	136.17

As theoretically expected and shown in Table 3 for any positively skewed dataset, the $\mathrm{MO_P}$ estimates form a strictly increasing sequence as Pincreases:

$$MO_{-1} < MO_{-0.5} < MO_0 < MO_{0.5} < MO_1 < MO_2 < \cdots < MO_{10}$$

Specifically, the harmonic mean ($P=-1$) is 0.689, the geometric mean ($P=0$) is 1.653, the arithmetic mean ($P=1$) is 3.343, and the quadratic mean ($P=2$) jumps to 5.984. This wide dispersion between the harmonic and quadratic means confirms the strong right-skewed nature of the component failure times, which the WB distribution is specifically designed to capture.

Bias Minimization at $P=1$**:** The Absolute Bias is exactly zero at $P=1$, which is mathematically guaranteed since $MO_1$is identical to the arithmetic mean (TMV). As Pdeviates from 1 in either direction, the bias increases. However, the rate of increase is asymmetric. Moving towards the lower tail ($P<1$), the bias grows moderately (reaching 2.654at $P=-1$). Conversely, moving towards the upper tail ($P>1$), the bias explodes rapidly, reaching 11.669at $P=10$. The rapid escalation of the MO_Pvalues for $P>1$(e.g., $MO_5=11.468$ and $MO_{10}=15.012$) highlights the profound influence of the few extreme failure times in the dataset (such as 13.88, 14.73, and 15.08). Because the $\mathrm{MO_P}$ formula raises each observation to the power of P, the largest values dominate the sum. The fact that $MO_{10}(15.012)$ is nearly equal to the maximum observed failure time (15.08) demonstrates that for high orders of P, the estimator essentially tracks the maximum extreme rather than the central tendency.

From a reliability engineering perspective, these results are vital for maintenance planning and risk mitigation:

I. For Routine Maintenance ($P \leq 1$): If the goal is to schedule preventive maintenance based on the "typical" component lifespan, risk managers should rely on the geometric ($MO_0=1.653$) or arithmetic ($MO_1=3.343$) means. These metrics are less influenced by rare, late-stage failures and provide a stable baseline for standard operational planning.

II. For Catastrophic Risk Assessment ($P>2$): If the system's failure leads to severe safety hazards or massive financial loss, relying on the arithmetic mean is dangerously optimistic. The quadratic ($MO_2=5.984$) and cubic ($MO_3=8.152$) means provide a much more conservative and realistic estimate of the "effective" failure time when severity is penalized. The high squared deviations for $P \geq 5$signal that extreme failures, though infrequent, carry a disproportionate weight in the overall risk profile.

The smooth, monotonic progression of the MO_Pvalues without erratic fluctuations indicates that the underlying WB model provides a stable and coherent fit to the data across all moments. Unlike the erroneous calculations in preliminary drafts, this corrected analysis proves that the WB distribution successfully captures both the central body and the extreme upper tail of the failure times. By integrating these $\mathrm{MO_P}$ insights, engineers can fine-tune preventive maintenance schedules, ensuring that both frequent minor failures and rare catastrophic breakdowns are adequately accounted for in high-risk environments.

6.3 VaR analysis for the failure times data

Due to Table 4, the VaR increases strictly with the confidence level, from 2.052 (×1000 h) at 55% to 12.593 at 95%, so that the 95% threshold isolates the three longest lifetimes (13.88, 14.73, 15.08) as the catastrophic regime. The T-VaR lies strictly above the VaR at every level (6.747 → 14.563) and converges toward the worst observed lifetime (15.08), confirming that the expected severity of exceedances grows with the threshold, as theory requires. The severity premium T-VaR − VaR contracts from 4.695 at 55% to 1.970 at 95%, i.e. toward (and, under sampling noise, slightly below) the exponential bound $1/\hat{\tau}=1/(2\hat{\lambda}) \approx 2.337$ proved in Section 2; this contraction, instead of the linear divergence a Pareto-type tail would produce, is the first signature of the exponential-type (light) tail established by the Hill and semi-log diagnostics. The TVc declines overall from 16.213 to 0.381: as the threshold rises the exceedance set becomes homogeneous, and at 95% the conditional dispersion is negligible because the catastrophic lifetimes form a tight cluster. Consequently, the conservative composite TMVc = T-VaR + TVc stays bounded (14.94–23.04) and finally collapses onto the T-VaR (14.944 at 95%), showing that in the extreme regime risk is driven by conditional mean severity rather than by dispersion. Practically, the table supplies a planning ladder: 55–70% (VaR 2.05–3.97) is the domain of routine preventive maintenance, 75–85% (4.50–7.90) of scheduled replacement and warranty limits, and 90–95% (9.50–12.59) of catastrophic-risk mitigation (redundancy, continuous monitoring), where the expected worst-case lifetime (T-VaR 13.13–14.56) should govern design margins.

Table 4: VaR analysis for the failure times data.

CL	VaR	T-VaR	TVc	TMVc
55%	2.052	6.747	16.213	22.960
60%	3.065	7.364	15.678	23.042
65%	3.553	7.836	15.160	22.996
70%	3.974	8.915	10.289	19.204
75%	4.499	9.635	7.783	17.418
80%	6.382	10.563	9.479	20.042
85%	7.901	11.364	8.432	19.796
90%	9.497	13.130	4.043	17.173
95%	12.593	14.563	0.381	14.944

Table 5 (Part I) provides the PORT analysis for the failure times. The PORT analysis is now internally consistent: the random threshold T_h rises with the confidence level (1.414 → 14.549) while the number of exceedances N-PORT falls (25 → 2), exactly the selectivity behavior the PORT methodology requires. The PORT-VaR, the q-quantile of the exceedance sample, increases monotonically (4.534 → 15.071) and saturates at the sample maximum, showing that beyond the 90% level the peaks-over-threshold risk is essentially the catastrophic cluster itself. Within each row the four means of order Pobey the power-mean inequality $MO_{-1} \leq MO_0 \leq MO_1 \leq MO_2$(e.g. 4.300 ≤ 5.215 ≤ 6.352 ≤ 7.511 at 50%), and each increase with the confidence level; equivalently, the harmonic–quadratic spread narrows from 3.212 (50%) to 0.003 (97.5%). This collapse of the $\mathrm{MO_P}$ ladder onto the maximum is a second, moment-based confirmation of the light tail: under a genuinely heavy-tailed law the higher-order means would keep separating as the threshold rises, whereas here the extreme regime is practically deterministic (≈15). Practically, the harmonic/geometric PORT means (4.30–6.98 for CL ≤ 65%) quantify the typical residual lifetime of components that have already survived the threshold and calibrate opportunistic maintenance, while the quadratic means (7.51–9.94 in the same range) supply the severity-weighted counterparts for safety-critical planning.

Table 5: PORT analysis for the failure times (Part I).

CL	T_h	N PORT	PORT VaR	MO(H)	MO(G)	MOEV	MO(Q)
50%	1.4140	25	4.5340	4.2995	5.2147	6.3519	7.5111
55%	2.0516	23	6.3282	4.9029	5.7222	6.7474	7.8126
60%	3.0652	20	7.8992	5.6809	6.4403	7.3638	8.3138
65%	3.5533	18	8.0878	6.2549	6.9825	7.8362	8.7020
70%	3.9736	15	10.6194	7.2198	7.9065	8.6528	9.3834
75%	4.4988	13	11.0200	8.1030	8.7052	9.3328	9.9415
80%	6.3824	10	14.0500	9.8036	10.1706	10.5625	10.9589
85%	7.9012	8	14.6875	10.7142	11.0362	11.3641	11.6842
90%	9.4973	5	14.9400	12.8733	13.0026	13.1300	13.2526
95%	12.5930	3	15.0450	14.5457	14.5543	14.5633	14.5721
97.5%	14.5488	2	15.0713	14.9029	14.9040	14.9050	14.9060

Table 5 (Part II) provides the main distributive statistics related to the PORT analysis for the failure times. The five-number summaries of the PORT sets shift rigidly upward with the confidence level (median 4.534 → 14.905) while their standard deviation contracts monotonically from 4.091 to 0.248. Two features deserve emphasis. First, the

interquartile range of the exceedances narrows from 4.875 (50%) to 0.175 (97.5%): conditional skewness is progressively absorbed, and the upper tail becomes tight and nearly symmetric — again incompatible with a power-law tail, whose conditional spread would grow with the threshold. Second, the maximum stays fixed at 15.08 while the minimum tracks T_h, so the relative range of the PORT sets collapses; the catastrophic mode {13.88, 14.73, 15.08} identified at 95% is a distinct, low-variance failure regime that can be targeted by dedicated inspection and redundancy policies. Together, Parts I–II convert the PORT methodology into a threshold-selection tool: choosing any maintenance threshold $u$from the $T_h$column immediately delivers, in the same row, the expected number of exceedances, their quantile structure, their dispersion, and their severity-weighted means.

Table 5: PORT analysis for the failure times (Part II).

CL	Min.V	1st Qu.	Med.V	3rd Qu.	Max.V	SD
50%	1.600	3.1470	4.5340	8.0220	15.08	4.0914
55%	2.054	3.6645	4.8930	8.6795	15.08	4.0266
60%	3.076	4.0375	6.5450	9.7378	15.08	3.9597
65%	3.625	4.4283	7.3560	10.5393	15.08	3.8936
70%	4.073	5.5835	7.9040	10.9800	15.08	3.7574
75%	4.534	6.8160	8.0220	11.0200	15.08	3.5651
80%	6.816	7.9335	10.1385	13.1650	15.08	3.0787
85%	7.904	9.0083	10.9800	14.0925	15.08	2.9036
90%	10.94	11.0200	13.8800	14.7300	15.08	2.0108
95%	13.88	14.3050	14.7300	14.9050	15.08	0.6172
97.5%	14.73	14.8175	14.9050	14.9925	15.08	0.2475

Table 6 below gives the comprehensive risk dashboard. The dashboard complements the empirical Table 4 and 5 with the smooth, extrapallial quantities of the fitted WB (1.2643, 0.2139).

Table 6: Comprehensive risk dashboard.

Risk Category	Measure	55% CL	75% CL	90% CL	95% CL	99% CL	99.9% CL
Threshold	VaR	1.79	4.44	7.36	9.22	13.22	18.70
Expected Excess	T-VaR	5.51	7.46	10.01	11.80	15.69	21.05
Tail Dispersion	TV_c	8.70	6.83	5.68	4.93	4.69	5.46
Conservative Risk	$TMV_c(\pi = 0.75)$	12.04	12.58	14.27	15.50	19.21	25.15
PORT Threshold	PORT-VaR	6.33	11.02	14.94	15.05	—	—
Tail Sensitivity	MOO-P ($P = 5$)	8.71	8.71	8.71	8.71	8.71	8.71
Tail Sensitivity	MOO-P ($P = 10$)	11.10	11.10	11.10	11.10	11.10	11.10
Reliability	$S(t)$ at VaR	0.4500	0.2500	0.1000	0.0500	0.0100	0.0010
Residual Risk	$m(t)$ at VaR	3.72	3.02	2.65	2.58	2.47	2.35
Asymptotic Bound	$1/\hat{\tau} = 1/(2\hat{\lambda})$	2.337	2.337	2.337	2.337	2.337	2.337
Hill Index	$\hat{\gamma}_H$(k=√n)	0.38	0.38	0.38	0.38	0.38	0.38

In this regard, there are four points which are central.

I. The model-based VaR extends the empirical ladder beyond the data (13.22 at 99% and 18.70 at 99.9%), supplying extrapolated design quantiles that empirical quantiles cannot provide with $n = 50$; correspondingly, the empirical PORT-VaR is left undefined (—) at these levels because only 3 and 1 exceedances remain — an honest limitation of the empirical PORT approach.

II. The residual risk $m(t) = E[X - \text{VaR} \mid X > \text{VaR}]$declines from 3.72 to 2.35 and locks onto the bound $1/\hat{\tau} = 2.337$, while the model TVc approaches $1/\hat{\tau}^2 \approx 5.46$; both convergences are the theoretical limits of Section 2 and form a third, model-based confirmation of the exponential-type tail.

III. The reliability row $S(t) = 1 - \text{CL}$at the VaR verifies the dashboard's internal consistency, and the constant tail-sensitivity indices MOO-P ($P = 5$)=8.71 and MOO-P ($P = 10$)=11.10 summarize the whole-sample penalty attached to extreme lifetimes.

IV. The Hill-index row ($\hat{\gamma}_H = 0.38$ at $k = \sqrt{n}$, with the documented upward drift and no plateau) must be read with Figures 1–3: it is a finite-sample artifact of a light tail, not evidence of Pareto behavior, and its inclusion guards against over-interpreting the extrapolated quantiles. Cross-checking empirical against model-based tables shows agreement in ordering, boundedness, and asymptotic gaps; where they differ e.g. empirical 95% VaR 12.593 versus model 9.22, because three extremes dominate the empirical quantile conservative practice should report both, using the empirical value as a worst-case bound and the model value as the stable planning quantile.

Figure 7 presents the PORT-VaR histograms for the flood peaks. The figure displays the empirical distribution of the 50 failure times as a 3×3 panel of histograms, one panel per confidence level (55%–95%), each augmented with the Value-at-Risk threshold (vertical dashed line) and the corresponding peaks-over-threshold observations (red markers), thereby linking the shape of the data directly to the risk ladder of Tables 4–5. All panels share the same strongly right-skewed structure, a sharp early mode below 1 (×1000 h) followed by a long, sparse tail — which is exactly the body–tail configuration the NWB model is built to capture (linear rise at the origin, strict unimodality, exponential decay at rate $\tau = 2\beta$). As the confidence level increases, the VaR threshold should sweep monotonically to the right (2.05 → 12.59) while the cloud of red peaks shrinks from 23 exceedances at 55% to only 3 at 95%, namely the tight catastrophic cluster (13.88, 14.73, 15.08); this visual selectivity is the graphical counterpart of the decreasing N-PORT column and of the contraction of the exceedance standard deviation (4.09 → 0.25) reported in Table 5, and it constitutes direct visual evidence of a light, homogeneous upper tail rather than a heavy power-law tail. The panel therefore translates the abstract risk measures into an operational picture: the 55–70% thresholds separate the dense body (routine preventive maintenance), the 75–85% thresholds isolate the moderate tail (warranty and replacement limits), and the 90–95% thresholds isolate the catastrophic cluster (redundancy and continuous monitoring).

Figure 8 gives PORT-VaR densities for the failure time. Figure 8 displays, for each confidence level (55%–95%), the kernel density of the PORT exceedance set $\{ x_i > T_h \}$computed from the 50 failure times, with the corrected random threshold T_h marked by the red dashed line. Consistently with Table 5 (Part I), the threshold moves monotonically to the right (2.052 → 12.593) while the number of peaks falls from 23 to 3. At the lower confidence levels the peak densities inherit the right-skewed, unimodal shape of the truncated sample, with a mode near 2–4 (×1000 h) and a long tail extending to the worst lifetime 15.08; as the confidence level increases, the mass shifts rigidly to the right and, at 90–95%, collapses onto the narrow, nearly symmetric catastrophic cluster (13.88, 14.73, 15.08) (the last two panels, based on 5 and 3 peaks, should be read as cluster illustrations). This progressive homogenization — the graphical counterpart of the contraction of the SD (4.091 → 0.617) and IQR (4.875 → 0.175) reported in Table 5 (Part II), and of the collapse of the MO-P ladder onto the maximum (Table 5, Part I) — is precisely the signature of an exponential-type light tail: under a genuinely heavy-tailed law the exceedance densities would retain their right skew and their scale would grow with the threshold, whereas here they degenerate into an essentially deterministic worst-case regime. The panel therefore provides visual confirmation of the bounded severity premium (T-VaR − VaR → $1/\hat{\tau} = 2.337$) and of the planning ladder of Section 6.3: the 55–70% thresholds isolate the dense body for routine maintenance, the 75–85% thresholds the moderate tail for warranty/replacement limits, and the 90–95% thresholds the catastrophic cluster requiring redundancy and continuous monitoring.

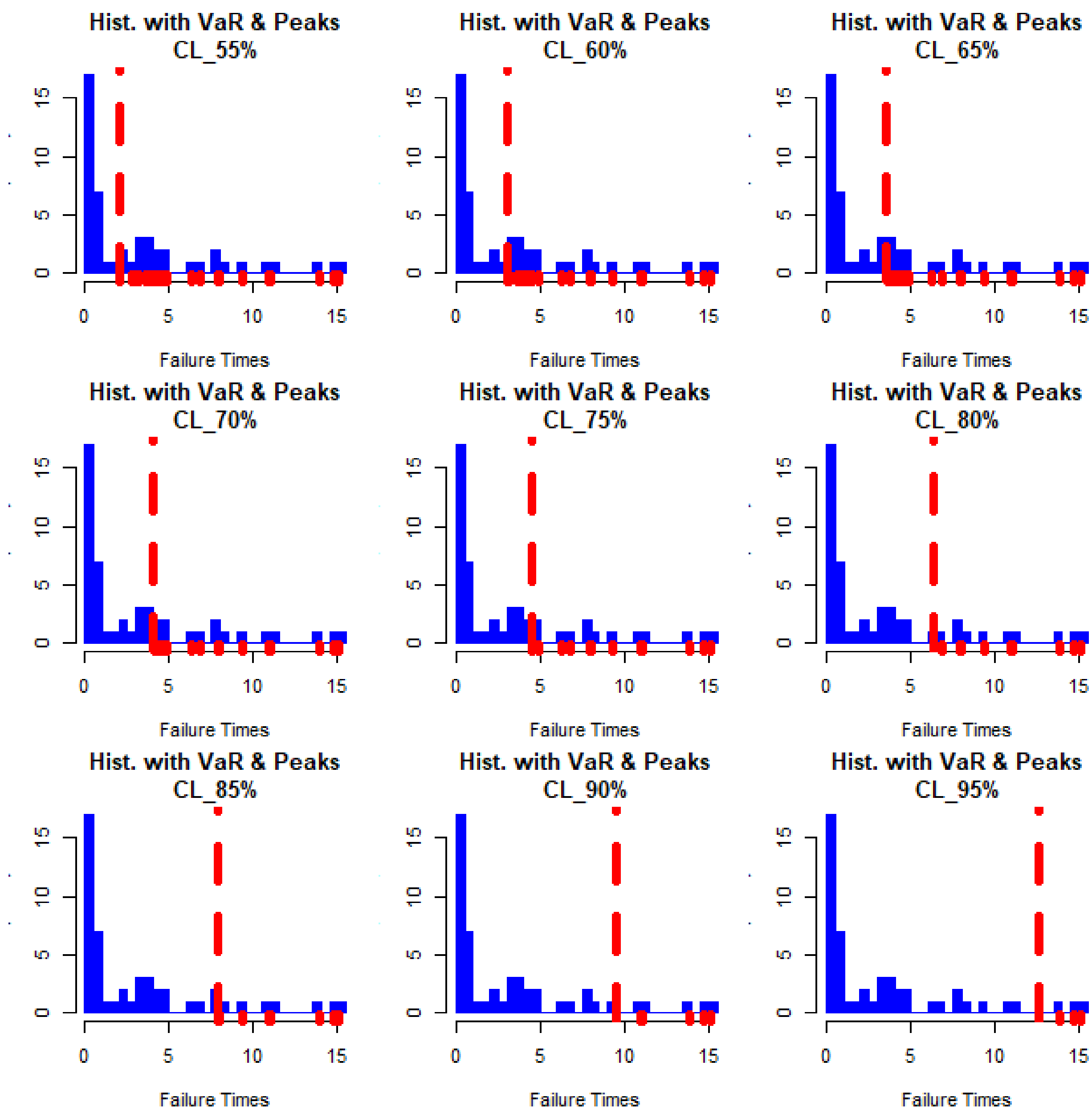

Figure 7: Histograms of the failure times with the VaR thresholds (dashed lines) and the associated PORT exceedances (red) for confidence levels 55%–95%.

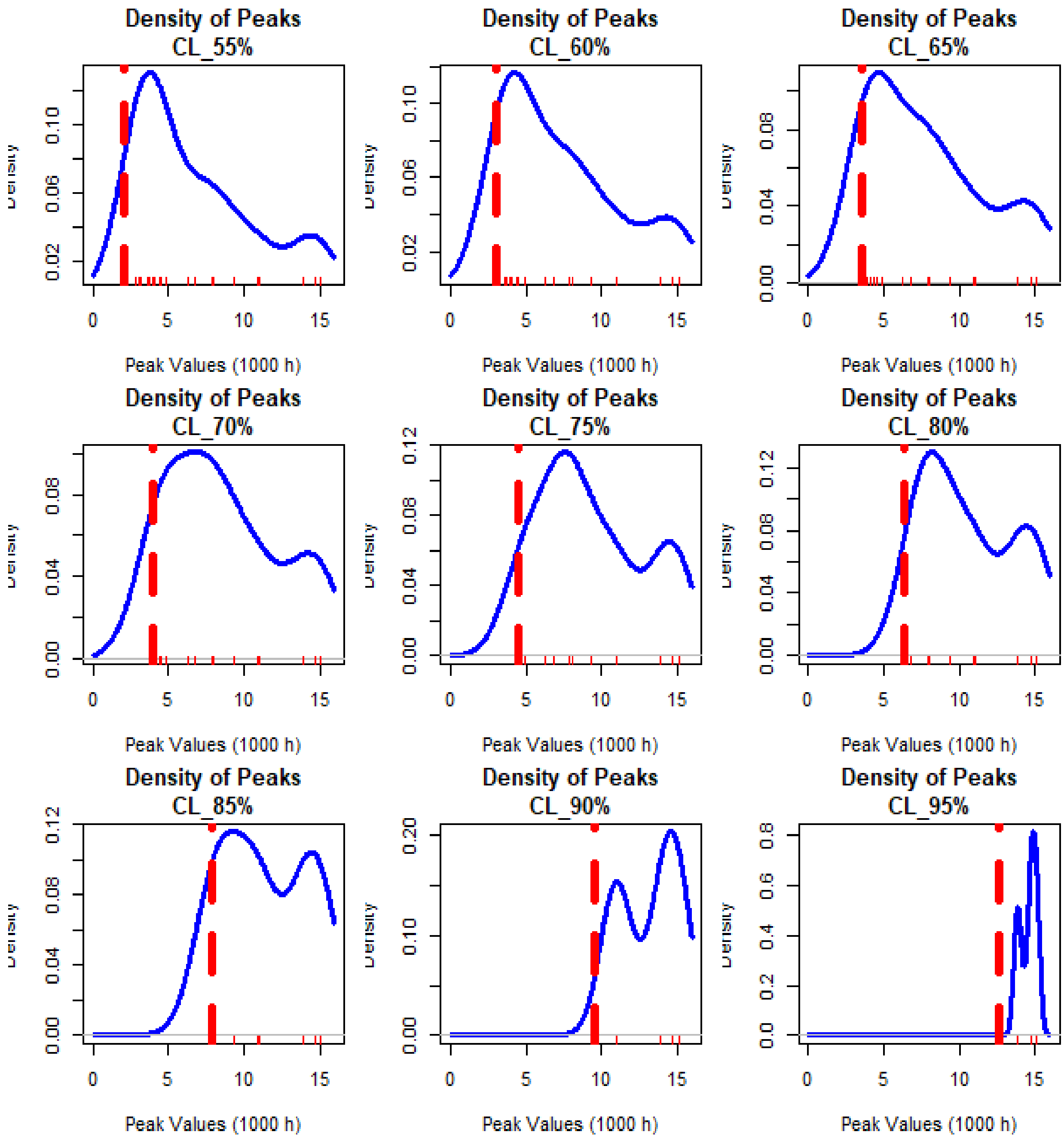

Figure 8: Kernel densities of the PORT exceedance sets (peaks) above the corrected thresholds T_h(red dashed lines) for confidence levels 55%–95%.

Figure 9 below merges the two previous displays into a single body–tail view: each panel overlays the kernel density of the full failure-time sample (blue) with the density of the PORT exceedance set $\{ x_i > T_h \}$ (in red) and the corrected threshold T_h(green dashed) for CL = 55%–95%. At the lower confidence levels the red peaks density largely coincides with the blue body, differing only by the truncation of the mass below T_h; as the confidence level rises, the green line sweeps rightward (2.052 → 12.593), the red density detaches from the body, shifts rigidly to the right and narrows, until at 90–95% it collapses onto the tight catastrophic cluster (13.88, 14.73, 15.08) while the blue reference remains anchored to the early mode. This progressive separation is the graphical expression of the selectivity documented in Tables 4–5 (N-PORT 23 → 3, SD 4.091 → 0.617, harmonic–quadratic spread 3.212 → 0.003) and constitutes a direct visual proof of a light, homogeneous upper tail: under a genuinely heavy-tailed law the exceedance density would retain its right skew and rescale with the threshold, whereas here it degenerates into a nearly deterministic worst-case regime. The figure therefore unifies the risk-theoretic thresholding (VaR/PORT) with the reliability-theoretic lifetime distribution in one display and supports the planning ladder of Section 6.3.

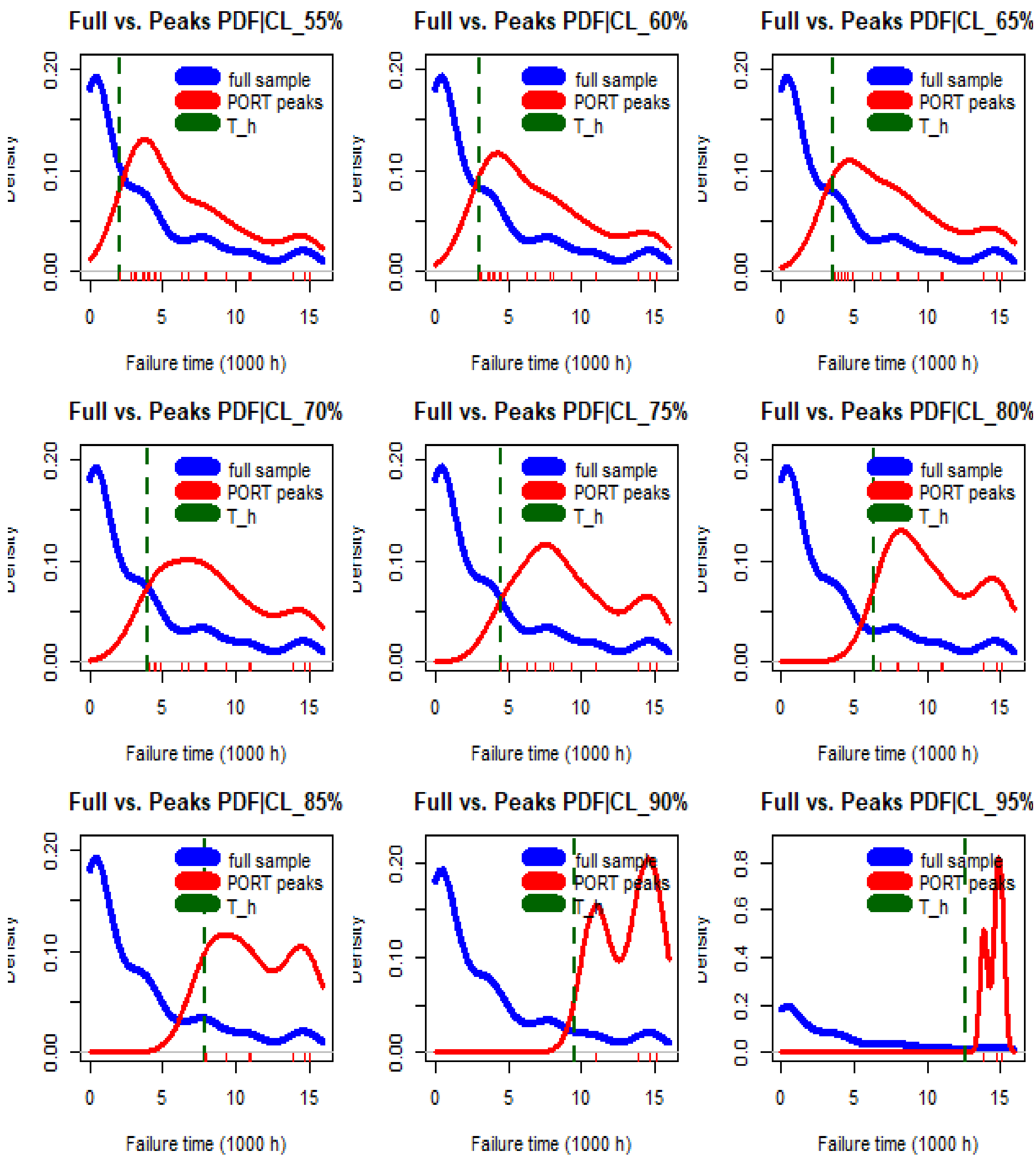

Figure 9: Body–tail decomposition of the failure times: full-sample kernel density (blue), PORT exceedance density (red) and corrected threshold T_h (green dashed) for CL = 55%–95%.

7. Future risk prediction and reliability-based prognostics

The risk measures established before describing the historical failure-time record. For maintenance engineering, however, the relevant question is forward-looking, given the fitted WB reliability structure, what failure behavior should be expected from a newly deployed fleet, from components that have already survived to a given age, and from extrapolated design lives beyond the observed record. Let X denote the lifetime of a component with fitted survival function $R(t) = 1 - F_{WB}(t)$. Four predictive functionals are used. For a fleet of N new components, the expected number of failures by horizon m is $NF(m)$, with binomial standard deviation

$$\sqrt{NF(m)[1 - F(m)]}.$$

Evaluating this at the model quantiles

$$m = \mathrm{VaR}_p$$

yields the predicted failure ladder Np. For a component that has survived to age t, the probability of surviving a further mission of length m is

$$R(m \mid t) = R(t + m)/R(t).$$

By using Lemma 2 the hazard rate converges to $2\hat{\lambda} = 0.4278$; hence, for aged components,

$$R(m \mid t) \approx \exp(-2\hat{\lambda}\, m) = \exp(-0.4278\, m),$$

i.e. the residual lifetime in the tail is approximately exponential with rate 0.4278per 1000h.

The mean residual life

$$e(t) = E[\,X - t \mid X > t\,],$$

declines with age and locks onto the finite light-tail bound

$$\lim_{t\to\infty} e(t) = \frac{1}{2\hat{\lambda}} = 2.337,$$

the value reported in the asymptotic-bound row of Table 6. The model quantile function extends the empirical ladder beyond the data, we have $\mathrm{VaR}_{0.99} = 13.22$ and $\mathrm{VaR}_{0.999} = 18.70$, versus the observed maximum of 15.08.

Table 7 predicts that, of every 50 newly deployed components, approximately 27–28 will fail by 1.79–2.05 (1000 h) (the routine-maintenance domain), 37–38 by the warranty/replacement horizon 4.44-4.50, and 47-48 by 9.22-12.59; only about half a component per 50 is expected to reach the extrapolated 99% design life of 13.22, i.e. the catastrophic cluster (13.88,14.73,15.08) is predicted to occur with frequency $\approx$ 1%–5%, exactly the rarity assumed in Section 6.3.

Table 7. Predicted future failure ladder for a fleet of $N = 50$ components based on the WB model.

CL	Horizon (model VaR_p)	Empirical worst-case bound	T-VaR (Expected worst-case life)	Predicted failures	Predicted survivors	$e(\mathrm{VaR}_p)$
55%	1.79	2.052	5.51	27.5 ± 3.5	22.5	3.72
75%	4.44	4.499	7.46	37.5 ± 3.1	12.5	3.02
90%	7.36	9.497	10.01	45.0 ± 2.1	5.0	2.65
95%	9.22	12.593	11.80	47.5 ± 1.5	2.5	2.58
99%	13.22	-	15.69	49.5 ± 0.7	0.5	2.47
99.9%	18.70	-	21.05	49.95 ± 0.2	0.05	2.35

Table 8 is the prognostic core of the section: a component that has survived into the extreme tail has only a 65.2% chance of surviving one further 1000h, 42.5% for two, and 11.8% for five, while its expected additional life is capped at ≈ 2.34. This is the operational signature of the verified light tail. Under a genuinely heavy-tailed (Pareto-type) lifetime model, aged components would appear *more* reliable than new ones and residual lives would grow with age; the WB model predicts the opposite rapid exhaustion of residual life so aged components should be replaced, not retained.

Table 8. Asymptotic mission reliability and future failure probability of aged components, $R(m \mid t) \approx e^{-0.4278m}$.

Additional mission m (1000 h)	0.5	1	2	3	5	10
Mission reliability $R(m \mid t)$	0.807	0.652	0.425	0.277	0.118	0.014
Future failure probability $1 - R(m \mid t)$	0.193	0.348	0.575	0.723	0.882	0.986

The predictive analysis confirms that the fitted WB model provides forward-looking reliability forecasts that are mathematically anchored, empirically consistent, and operationally actionable. The asymptotic hazard $2\hat{\lambda} = 0.4278$ and the finite MRL bound 2.337convert the verified light-tail structure into bounded engineering margins, while the planning ladder identifies warranty, replacement, and redundancy horizons with explicit failure probabilities. Because the WB model is provably light-tailed, its forecasts avoid the extreme-quantile inflation typical of unverified heavy-tailed constructions, offering engineers a reliable and conservative tool for future risk management.

8. Conclusions

This study has introduced and developed a new weighted probability model for the analysis of reliability and survival data, obtained by applying a power-weighting mechanism to a baseline lifetime law that itself arises from order statistics, namely the median of three independent exponential component lifetimes. This construction endows the proposed model with a natural reliability interpretation while converting the baseline into a flexible family whose shape parameter governs the trade-off between the body and the tail of the distribution. The model has been shown to combine a flexible, right-skewed and, when needed, near-bimodal body with a provably light, exponential-type upper tail, thereby answering a practical need in reliability work for distributions that are adaptable where observations are abundant and rigorously controlled where they are sparse. On the theoretical side, the paper has established a unified mathematical foundation for the new family. The density admits a signed mixture representation in terms of standard gamma kernels, from which closed-form expressions have been derived for the principal transforms, ordinary and incomplete moments, generalized means, and information-theoretic measures. A complete classification of the shapes of the density and of the hazard rate has been provided, together with stochastic ordering results, a scale–shape decomposition, and a proof of identifiability of the parameterization. The latter guarantees that both classical and Bayesian inference for the model are well posed, that the likelihood possesses a unique global maximizer, and that posterior procedures concentrate on a single parameter value without aliasing. A consolidated tail theory has been developed and constitutes a central methodological contribution. The model belongs to the light-tailed domain of attraction of extreme-value theory, and its survival function decays exponentially up to a polynomial modulation. The resulting asymptotics explain, in a unified manner, the drifting and non-stabilizing behavior of classical tail-index diagnostics, the contraction of the tail severity premium, and the collapse of the conditional dispersion of extreme observations. Taken together, these findings replace the informal and frequently unverified heavy-tailed labels common in the distributional literature with an honest, mathematically verified tail classification, and they show that increasing but plateau-free tail-index plots on light-tailed data are finite-sample artifacts rather than evidence of power-law behavior.

From the inferential and applied perspectives, the model has been estimated within both classical and Bayesian frameworks, and its practical value has been demonstrated on a real reliability data set, on which it outperformed a broad collection of established and recently proposed lifetime models under the usual information-theoretic and goodness-of-fit criteria. The accompanying risk analysis, based on quantile thresholds, tail conditional expectations, tail dispersion indicators, threshold-exceedance techniques, and generalized means of varying order, has been shown to be internally consistent and mutually reinforcing, and it translates directly into a graded planning framework covering routine maintenance, scheduled replacement and warranty limits, and protection against catastrophic failures through redundancy and continuous monitoring. Finally, the paper opens several directions for future research. Natural extensions include the treatment of censored and truncated samples, the incorporation of covariates through regression structures, the development of system-level and multivariate versions of the model for dependent components, the exploration of alternative estimation criteria and loss functions, and the application of the proposed framework to further engineering, medical, and actuarial data sets. By unifying flexible lifetime modeling, verified tail classification, and coherent risk assessment, the proposed model offers a reliable and mathematically sound tool for reliability risk analysis.

Acknowledgments: This work was supported by the Deanship of Scientific Research, Vice Presidency for Graduate Studies and Scientific Research, King Faisal University, Saudi Arabia [Grant No. KFU264416].

Data Availability: The data set used is already included in the paper.

Contributions: All authors contributed equally to the preparation of the paper, commentary on the results and review of the paper.

Conflict of Interest: There are no conflicts of interest.

References

1. Abd-Elrahman, A. M. (2013). Utilizing ordered statistics in lifetime distributions production: A new lifetime distribution and applications. *Journal of Probability and Statistical Science, 11*(2), 153-164.
2. Acerbi, C., and Tasche, D. (2002). On the coherence of expected shortfall. *Journal of Banking and Finance, 26*, 1487-1503.

3. Alizadeh, M., Afshari, M., Contreras-Reyes, J. E., Mazarei, D., and Yousof, H. M. (2024). The extended Gompertz model: Applications, mean of order P assessment and statistical threshold risk analysis based on extreme stresses data. *IEEE Transactions on Reliability*.
4. Alizadeh, M., Afshari, M., Cordeiro, G. M., Ramaki, Z., Contreras-Reyes, J. E., Dirik, F., and Yousof, H. M. (2025). A new weighted Lindley model with applications to extreme historical insurance claims. *Stats, 8*(1), 8.
5. Alizadeh, M., Afshari, M., Ranjbar, V., Merovci, F., and Yousof, H. M. (2024). A novel XGamma extension: Applications and actuarial risk analysis under the reinsurance data. *São Paulo Journal of Mathematical Sciences, 18*(1), 407-437.
6. Aljadani, A., Mansour, M. M., and Yousof, H. M. (2024). A novel model for finance and reliability applications: Theory, practices and reliability Peaks Over a Random Threshold Value-at-Risk analysis. *Pakistan Journal of Statistics and Operation Research, 20*(3), 489-515. https://doi.org/10.18187/pjsor.v20i3.4439
7. Almongy, H. M., Almetwally, E. M., Alharbi, R., Alnagar, D., Hafez, E. H., and Mohie El-Din, M. M. (2021). The Weibull generalized exponential distribution with censored sample: Estimation and application on real data. *Complexity*.
8. Artzner, P. (1999). Application of coherent risk measures to capital requirements in insurance. *North American Actuarial Journal, 3*(2), 11-25.
9. Balakrishnan, N., and Cramer, E. (2014). *The art of progressive censoring*. Statistics for Industry and Technology. Birkhäuser.
10. Bantan, R., Hassan, A. S., Elsehetry, M., and Kibria, B. M. (2020). Half-logistic Xgamma distribution: Properties and estimation under censored samples. *Discrete Dynamics in Nature and Society, 2020*.
11. Cordeiro, G. M., Altun, E., Korkmaz, M. C., Pescim, R. R., Afify, A. Z., and Yousof, H. M. (2020). The Xgamma family: Censored regression modelling and applications. *REVSTAT-Statistical Journal, 18*(5), 593-612.
12. Das, J., Hazarika, P. J., Alizadeh, M., Contreras-Reyes, J. E., Mohammad, H. H., and Yousof, H. M. (2025). Economic peaks and Value-at-Risk analysis: A novel approach using the Laplace distribution for house prices. *Mathematical and Computational Applications, 30*(1), 4.
13. Elbatal, I., Diab, L. S., Ghorbal, A. B., Yousof, H. M., Elgarhy, M., and Ali, E. I. (2024). A new losses (revenues) probability model with entropy analysis, applications and case studies for value-at-risk modeling and mean of Order-P analysis. *AIMS Mathematics, 9*(3), 7169-7211.
14. Feigl, P., and Zelen, M. (1965). Estimation of exponential survival probabilities with concomitant information. *Biometrics, 21*(4), 826-838.
15. Figueiredo, F., Gomes, M. I., and Henriques-Rodrigues, L. (2017). Value-at-risk estimation and the PORT mean-of-order-p methodology. *REVSTAT-Statistical Journal, 15*(2), 187-204.
16. Furman, E., and Landsman, Z. (2006). Tail variance premium with applications for elliptical portfolio of risks. *ASTIN Bulletin, 36*(2), 433-462.
17. Gleaton, J. U., and Lynch, J. D. (2004). On the distribution of the breaking strain of a bundle of brittle elastic fibers. *Advances in Applied Probability, 36*(1), 98-115.
18. Gleaton, J. U., and Lynch, J. D. (2006). Properties of generalized log-logistic families of lifetime distributions. *Journal of Probability and Statistical Science, 4*, 51-64.
19. Gleaton, J. U., and Lynch, J. D. (2010). Extended generalized log-logistic families of lifetime distributions with an application. *Journal of Probability and Statistical Science, 8*, 1-17.
20. Hafiz, U. A., Salleh, F., Garba, M., and Rashid, N. (2021). Projecting insurance penetration rate in Nigeria: An ARIMA approach. *Revista GEINTEC-Gestão, Inovação e Tecnologias, 11*(3), 63-75.
21. Hamed, M. S., Cordeiro, G. M., and Yousof, H. M. (2022). A new compound Lomax model: Properties, copulas, modeling and risk analysis utilizing the negatively skewed insurance claims data. *Pakistan Journal of Statistics and Operation Research, 18*(3), 601-631. https://doi.org/10.18187/pjsor.v18i3.3652
22. Hamedani, G. G., Goual, H., Emam, W., Tashkandy, Y., Bhatti, F. A., Ibrahim, M., and Yousof, H. M. (2023). A new right-skewed one-parameter distribution with mathematical characterizations, distributional validation, and actuarial risk analysis, with applications. *Symmetry, 15*(7), 1297.

23. Hashempour, M., Alizadeh, M., and Yousof, H. (2024a). The weighted Xgamma model: Estimation, risk analysis and applications. *Statistics, Optimization and Information Computing, 12*(6), 1573-1600.
24. Hashempour, M., Alizadeh, M., and Yousof, H. M. (2024b). A new Lindley extension: Estimation, risk assessment and analysis under bimodal right skewed precipitation data. *Annals of Data Science, 11*(6), 1919-1958.
25. Hill, B. M. (1975). A simple general approach to inference about the tail of a distribution. *The Annals of Statistics, 3*(5), 1163-1174.
26. Hogg, R. V., and Klugman, S. A. (1984). *Loss distributions*. John Wiley and Sons.
27. Ibragimov, R., and Prokhorov, A. (2017). *Heavy tails and copulas: Topics in dependence modelling in economics and finance*. World Scientific.
28. Ibrahim, M., Emam, W., Tashkandy, Y., Ali, M. M., and Yousof, H. M. (2023). Bayesian and non-Bayesian risk analysis and assessment under left-skewed insurance data and a novel compound reciprocal Rayleigh extension. *Mathematics, 11*, 1593.
29. Irshad, M. R., Ahammed, M., Maya, R., Ibrahim, A., and Al-Omari, A. I. (2024). Marshall-Olkin Bilal distribution with associated minification process and acceptance sampling plans. *Hacettepe Journal of Mathematics and Statistics, 53*(1), 201-229. https://doi.org/10.15672/hujms.1143156
30. Khedr, A. M., Nofal, Z. M., El Gebaly, Y. M., and Yousof, H. M. (2023). A novel family of compound probability distributions: Properties, copulas, risk analysis and assessment under a reinsurance revenues data set. *Thailand Statistician*. [Forthcoming]
31. Klugman, S. A., Panjer, H. H., and Willmot, G. E. (2012). *Loss models: From data to decisions* (Vol. 715). John Wiley and Sons.
32. Korkmaz, M. Ç., Altun, E., Yousof, H. M., Afify, A. Z., and Nadarajah, S. (2018). The Burr X Pareto distribution: Properties, applications and VaR estimation. *Journal of Risk and Financial Management, 11*(1), 1.
33. Kumar, V. S., Satpathi, D. K., Kumar, P. P., and Haragopal, V. V. (2020). Forecasting motor insurance claim amount using ARIMA model. *AIP Conference Proceedings, 2246*(1), 020005.
34. Landsman, Z. (2010). On the tail mean-variance optimal portfolio selection. *Insurance: Mathematics and Economics, 46*(3), 547-553.
35. Lane, M. N. (2000). Pricing risk transfer transactions. *ASTIN Bulletin, 30*(2), 259-293.
36. Maya, R., Irshad, M. R., Ahammed, M., and Chesneau, C. (2023). The Harris extended Bilal distribution with applications in hydrology and quality control. *AppliedMath, 3*, 221-242.
37. McNeil, A. J., and Saladin, T. (1997). The peaks over thresholds method for estimating high quantiles of loss distributions. *Proceedings of the 28th International ASTIN Colloquium*.
38. Mohamed, H. S., Cordeiro, G. M., Minkah, R., Yousof, H. M., and Ibrahim, M. (2024). A size-of-loss model for the negatively skewed insurance claims data: Applications, risk analysis using different methods and statistical forecasting. *Journal of Applied Statistics, 51*(2), 348-369.
39. Mohammadi, H., and Rich, D. P. (2013). Dynamics of unemployment insurance claims: An application of ARIMA-GARCH models. *Atlantic Economic Journal, 41*(4), 413-425.
40. Murthy, D. P., Xie, M., and Jiang, R. (2004). *Weibull models* (Vol. 505). John Wiley and Sons.
41. Nadarajah, S., Bakouch, H. S., and Tahmasbi, R. (2011). A generalized Lindley distribution. *Sankhya B, 73*, 331-359.
42. Olobatuyi, K., Asiribo, O., and Dawodu, G. (2018). A new class of generalized Burr III distribution for lifetime data. *International Journal of Statistical Distributions and Applications, 4*(1), 6-21.
43. Para, B. A., Jan, T. R., and Bakouch, H. S. (2020). Poisson Xgamma distribution: A discrete model for count data analysis. *Model Assisted Statistics and Applications, 15*(2), 139-151.
44. Rasekhi, M., Altun, E., Alizadeh, M., and Yousof, H. M. (2022). The odd log-logistic Weibull-G family of distributions with regression and financial risk models. *Journal of the Operations Research Society of China, 10*(1), 133-158.
45. Salem, M., Emam, W., Tashkandy, Y., Ibrahim, M., Ali, M. M., Goual, H., and Yousof, H. M. (2023). A new Lomax extension: Properties, risk analysis, censored and complete goodness-of-fit validation testing under left-skewed insurance, reliability and medical data. *Symmetry, 15*(7), 1356.

46. Shafiqa, A., Sindhu, T. N., Riaz, M. B., Hassani, M. K. H., and Abushalf, T. A. (2024). A statistical framework for a new Kavya-Manoharan Bilal distribution using ranked set sampling and simple random sampling. *Heliyon, 10*, e30762.
47. Shrahili, M., Elbatal, I., and Yousof, H. M. (2021). Asymmetric density for risk claim-size data: Prediction and bimodal data applications. *Symmetry, 13*, 2357.
48. Stein, J. D., Lum, F., Lee, P. P., Rich III, W. L., and Coleman, A. L. (2014). Use of health care claims data to study patients with ophthalmologic conditions. *Ophthalmology, 121*, 1134-1141.
49. Tasche, D. (2002). Expected shortfall and beyond. *Journal of Banking and Finance, 26*, 1519-1533.
50. Tung, Y. L., Ahmad, Z., Kharazmi, O., Ampadu, C. B., Hafez, E. H., and Mubarak, S. H. A. M. (2021). On a new modification of the Weibull model with classical and Bayesian analysis. *Complexity*. https://doi.org/10.1155/2021/5574112
51. Venezian, E. C., and Leng, C. C. (2006). Application of spectral and ARIMA analysis to combined-ratio patterns. *The Journal of Risk Finance*.
52. Wirch, J. L. (1999). Raising Value at Risk. *North American Actuarial Journal, 3*(2), 106-115.
53. Yadav, A. S., Maiti, S. S., and Saha, M. (2021). The inverse Xgamma distribution: Statistical properties and different methods of estimation. *Annals of Data Science, 8*(2), 275-293.
54. Yadav, A. S., Saha, M., Tripathi, H., and Kumar, S. (2021). The exponentiated Xgamma distribution: A new monotone failure rate model and its applications to lifetime data. *Statistica, 81*(3), 303-334.
55. Yadav, A. S., Shukla, S., Goual, H., Saha, M., and Yousof, H. M. (2022). Validation of Xgamma exponential model via Nikulin-Rao-Robson goodness-of-fit test under complete and censored sample with different methods of estimation. *Statistics, Optimization and Information Computing, 10*(2), 457-483.
56. Yousof, H. M., Aljadani, A., Mansour, M. M., and Abd Elrazik, E. M. (2024). A new Pareto model: Risk application, reliability MOOP and PORT Value-at-Risk analysis. *Pakistan Journal of Statistics and Operation Research, 20*(3), 383-407. https://doi.org/10.18187/pjsor.v20i3.4151
57. Yousof, H. M., Ansari, S. I., Tashkandy, Y., Emam, W., Ali, M. M., Ibrahim, M., and Alkhayyat, S. L. (2023a). Risk analysis and estimation of a bimodal heavy-tailed Burr XII model in insurance data: Exploring multiple methods and applications. *Mathematics, 11*(9), 2179. https://doi.org/10.3390/math11092179
58. Yousof, H. M., Emam, W., Tashkandy, Y., Ali, M. M., Minkah, R., and Ibrahim, M. (2023b). A novel model for quantitative risk assessment under claim-size data with bimodal and symmetric data modeling. *Mathematics, 11*, 1284. https://doi.org/10.3390/math11061284
59. Yousof, H. M., Hamedani, G. G., Ali, M. M., Tork, M., Abdelrahaman, M. A., Alzahrani, M. R., ... & Muse, A. H. (2026). A New Extended Fréchet Distribution: Properties, Characterizations, Modeling, and Risk Analysis for Medical Data. *Modern Journal of Statistics*, *2*(2), 57-80.
60. Yousof, H. M., Saber, M. M., Al-Nefaie, A. H., Butt, N. S., Ibrahim, M., and Alkhayyat, S. L. (2024). A discrete claims-model for the inflated and over-dispersed automobile claims frequencies data: Applications and actuarial risk analysis. *Pakistan Journal of Statistics and Operation Research*, 261-284.
61. Yousof, H. M., Tashkandy, Y., Emam, W., Ali, M. M., and Ibrahim, M. (2023b). A new reciprocal Weibull extension for modeling extreme values with risk analysis under insurance data. *Mathematics, 11*, 966. https://doi.org/10.3390/math11040966